



## 저작자표시-변경금지 2.0 대한민국

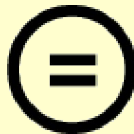
이용자는 아래의 조건을 따르는 경우에 한하여 자유롭게

- 이 저작물을 복제, 배포, 전송, 전시, 공연 및 방송할 수 있습니다.
- 이 저작물을 영리 목적으로 이용할 수 있습니다.

다음과 같은 조건을 따라야 합니다:



저작자표시. 귀하는 원저작자를 표시하여야 합니다.



변경금지. 귀하는 이 저작물을 개작, 변형 또는 가공할 수 없습니다.

- 귀하는, 이 저작물의 재이용이나 배포의 경우, 이 저작물에 적용된 이용허락조건을 명확하게 나타내어야 합니다.
- 저작권자로부터 별도의 허가를 받으면 이러한 조건들은 적용되지 않습니다.

저작권법에 따른 이용자의 권리는 위의 내용에 의하여 영향을 받지 않습니다.

이것은 [이용허락규약\(Legal Code\)](#)을 이해하기 쉽게 요약한 것입니다.

[Disclaimer](#)

2009. 08

Master's Thesis

**A Study on the Mechanical  
Characteristics in Dissimilar  
(Al / Mg) Alloy by using Friction  
Stir Welding**

Graduate School of Chosun University

Department of Naval Architecture and  
Ocean Engineering

Son Chang-Sik

# **A Study on the Mechanical Characteristics in Dissimilar (Al / Mg) Alloy by using Friction Stir Welding**

마찰교반용접을 이용한 이종합금재료(Al6061-T6 + AZ31)의  
기계적 특성에 관한 연구

August 2009

Graduate School of Chosun University

Department of Naval Architecture and  
Ocean Engineering

Son Chang-Sik

# **A Study on the Mechanical Characteristics in Dissimilar (Al / Mg) Alloy by using Friction Stir Welding**

Advisor : Professor Han-Sur Bang

A Thesis submitted for the degree of  
Master of Engineering

April 2009

Graduate School of Chosun University

Department of Naval Architecture and  
Ocean Engineering

Son Chang-Sik

## 孫昌植의 碩士學位 論文을 認准함

委員長 朝鮮大學校 教授 房 熙 善 \_\_\_\_\_

委 員 朝鮮大學校 教授 房 漢 瑞 \_\_\_\_\_

委 員 朝鮮大學校 教授 尹 德 榮 \_\_\_\_\_

2009 年 6 月 6 日

朝鮮大學校 大學院

## Contents

List of tables .....	iii
List of figures .....	iv
ABSTRACT.....	viii
 Chapter 1. Introduction .....	 1
1.1 The Background .....	1
1.2 The purpose .....	2
1.3 Method of study.....	6
1.3.1 Numerical Simulation .....	6
1.3.2 Experiment .....	8
 Chapter 2. Heat elasto–plastic theory and program .....	 9
2.1 Theory of Heat conduction analysis.....	9
2.2 Theory of thermal elasto–plastic analysis .....	13
2.3 Mathematic model for heat input .....	15
2.4 Flow chart of program .....	19
 Chapter 3. Numerical analysis of Friction Stir Welding..	23
3.1 Welding condition and analysis model .....	23
3.2 Temperature distribution .....	26
3.3 Residual stress distribution .....	28

Chapter 4. Experiment of Friction Stir Welding .....	29
4.1 FSW machine and tool shape .....	29
4.2 Welding condition and bead shape.....	31
4.2.1 Welding conditions .....	31
4.2.2 Bead shape .....	33
4.3 Experiment of stress measurement & mechanical properties of dissimilar welding .....	38
4.3.1 Welding residual stress .....	38
4.4 Mechanical property and micro-structure examination ..	41
4.4.1 Tension and Hardness test .....	42
4.4.2 Micro-structure examination by OM .....	49
4.4.3 Micro-structure examination by SEM and EDS ...	50
4.5 Consideration about experiment .....	53
 Chapter 5. Conclusion .....	 55
 REFERENCES .....	 57

## List of Tables

Table 3.1	Chemical compositions of Similar material .....	24
Table 3.2	Mechanical properties of Similar material .....	24
Table 3.3	Welding conditions .....	25
Table 4.1	List of welding condition .....	31
Table 4.2	Top bead shape .....	33
Table 4.4	Cross section of welding joints .....	50
Table 4.5	Micro-structure observation of condition number 52 .....	51
Table 4.6	Micro-structure observation of condition number 52 .....	52



## List of Figures

Fig. 1.1 Application of friction stir welding in industries.....	2
Fig. 1.2 Comparison of Friction Stir Welding with arc welding.....	3
Fig. 1.3 Schematic of Friction Stir Welding.....	4
Fig. 1.4 Typical model of the data transferring.....	7
Fig. 2.1 Flow pattern model of FSW.....	15
Fig. 2.2 Shoulder, Extrusion, Vortex zone height and width of extrusion for various rotations and translational speed of the tool.....	17
Fig. 2.3 Calculation for determination of the dimensions of the stir zone based on the Friction stir welding parameters.....	18
Fig. 2.4 Flow chart of the heat transfer analysis program.....	20
Fig. 2.5 Flow chart of the residual stress analysis program.....	20
Fig. 3.1 Model for numerical analysis.....	23
Fig. 3.2 Temperature relativity of mechanical properties.....	25
Fig. 3.3 Analysis model and mesh division .....	26
Fig. 3.4 Heat distribution with respect to time .....	27
Fig. 3.5 Contour of heat distribution in FSW .....	27
Fig. 3.6 Residual stress distribution .....	28
Fig. 4.1 FSW equipment and capacity .....	29
Fig. 4.2 Tool shape and drawing .....	30
Fig. 4.3 Specimen size .....	30
Fig. 4.4 Photograph of residual stress test specimens .....	39
Fig. 4.5 Residual stress measurement machine(XRD) .....	40
Fig. 4.6 Measurement points of welding residual stresses .....	40
Fig. 4.7 Measurement results of welding residual stress .....	41
Fig. 4.8 Photograph of tensile test specimen of similar & dissimilar Joint .....	43
Fig. 4.9 Analysis model and mesh division .....	44

Fig. 4.10 Strain–stress graph of tensile test .....	45
Fig. 4.11 Result graph of tensile test .....	46
Fig. 4.12 Photograph of vickers hardness test machine .....	47
Fig. 4.13 Measurement points of hardness test (HV) .....	47
Fig. 4.14 Result of hardness test specimen of dissimilar welded joint .....	48
Fig. 4.15 Photograph of macro–Structure of similar & dissimilar welded specimen .....	49

## ABSTRACT

# 마찰교반용접을 이용한 이종합금재료 (Al6061-T6 + AZ31)의 기계적 특성에 관한 고찰

조선대학교 대학원 선박해양공학과 손 창 식  
지 도 교 수 방 한 서

고도산업화에 따른 생산효율성의 증가는 기존의 비철금속의 영역을 더욱더 확장시켰으며, 그와 더불어 경량합금의 접합법 역시 중요한 산업기술의 요소로 부각되고 있다. 무엇보다 경량합금의 접합에 있어 크게 두각을 나타내는 마찰교반 접합법은 기존의 용접법에 비해서, 친환경적이며, 낮은 용접변형과 용접구조물의 강도적 측면에서 뛰어남이 여러 연구 논문에서 이미 입증된바 있다. 마찰교반 용접법의 영역은 빠르게 확대 되어가고 있으며, 접합대상이 기존의 마그네슘과 알루미늄 동종계의 경량합금에서 이종재의 경량합금의 접합 영역뿐 아니라 경합금과 철강재료의 접합의 영역까지 확대 되고 있다. 여기서 주목해야할 점은 마찰교반 용접법의 해석에 있어 일반적인 물리적인 실험이 대부분이며, 수치해석적인 측면에서의 이종 경합금간의 해석은 미흡한 단계이다.

그래서 본 연구에서는 알루미늄과 마그네슘 합금을 사용한 이종 재료의 접합을 수행하고 접합 기구를 규명하고자 하였으며, 더 나아가 마찰교반 용접부에서의 유동현상을 SEM과 EDS를 이용하여 보다 구체적으로 관찰하였다.

본 연구는 동종 및 이종 접합 시 내부의 역학적 거동을 고찰하기 위해 유한요소 해석을 수행하였으며, 이를 위해 열전도와 열탄소성 유한요소해석 프로그램을 개발하였다. 그리하여, 유한요소 해석에 의해 이종재질 간 용접 시 발생하는 열 이동현상과 이에 따른 응력의 발생특성을 명확하게 고찰할 수 있었으며, 또한, 알루미늄합금과 마그네슘 합금 간의 이종재질 접합에서 열분포 특성, 잔류응력 등을 고찰함으로써 입열에 의한 재료의 역학적 열화정도를 평가할 수 있었다.

## Chapter 1

### Introduction

Increase in productivity makes nonferrous metals to extend their use in production industries according to the high growth of industrialization. Welding methods suitable for joining nonferrous metals are also getting important with the development of industrial technology. Moreover, Friction stir welding focused in Mg alloys/Al alloys has proved to be predominance with the aspect of advantages concerning exhaust emissions, energy consumption, transport capacity and recycling material.

At present, FSW is being expanded to new areas in industries because of these advantages. In the past, FSW was used to join between Al and Al alloys, or AZ and AZ alloys. However, nowadays, it is being applied to join Steel and dissimilar alloys.

#### 1.1 Background

Friction stir welding is environmentally "friendly" method and FSW can join materials that are "unweldable" by fusion welding methods. FSW produces less distortion than fusion welding techniques, Friction stir welding uses a cylindrical, shouldered tool with a profiled pin that is rotated and slowly plunged into the joint line between two piece of sheet or plate material, which are butted together. Heat is generated in the stir zone of the work piece around the tool. This heat causes the work piece material to soften without reaching the melt in joint and allows the tool to traverse the weld line. As it does, the plasticized material is transferred from the leading edge of the tool to the trailing edge of the tool shoulder and pin. It leaves a solid phase bond between the two work pieces. Currently various research works are going on

in experimental aspects, numerical simulation and development of analytical solutions to describe the FSW process. But more detailed analytical models are still required to gain a clear physical insight of the friction stir welding process.

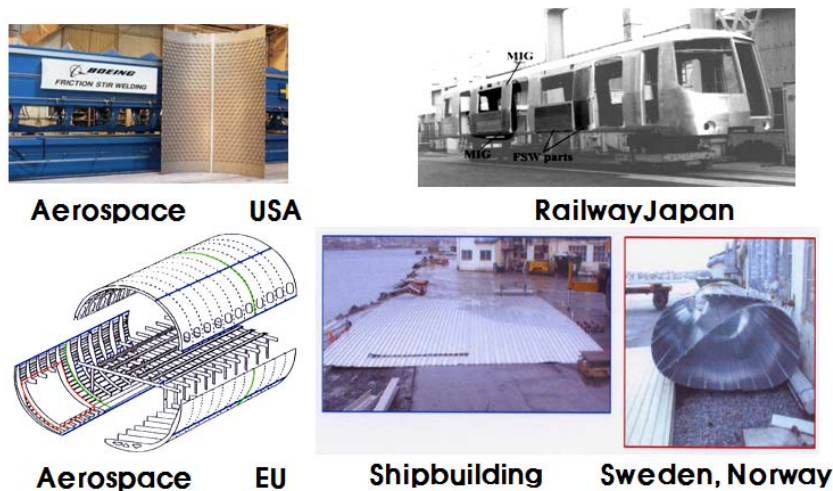


Fig. 1.1 Application of Friction Stir Welding in industries

## 1.2 The purpose

Through analysis of both similar and dissimilar welding joint, this study intends to examine the mechanical behavior, caused by FSW and change of residual stress, consequently obtain the mechanical properties and stability of the welding joint.

In order to achieve these purposes, the analysis of non-stationary heat conduction by finite element method was carried out. The effect of heat source and temperature dependency of physical coefficient (resistivity, heat conduction, specific heat and density and so on) is considered. Also the analysis of heat distribution and welding residual stresses by computing programme is used for numerical analysis which was performed considering the temperature dependency of mechanical properties(yield stress, elastic

coefficient and heat expansion coefficient and so on).

Moreover, this paper is to assess the welds of specimen and secure the mechanical phenomenon in welds experimentally and theoretically.

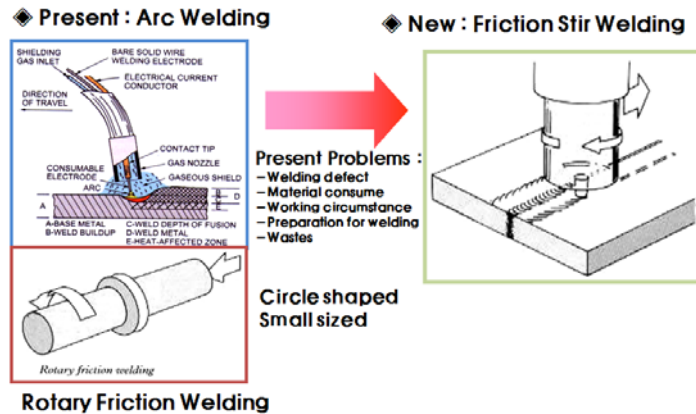


Fig. 1.2 Comparison of FSW with arc welding

### 1.2.1 Characteristics of Friction Stir Welding

Friction Stir Welding is a solid state joining method with five phases of actions in its entire process. The first is the plunging period, where the pin is fully and shoulder is partially plunged into the joint line of the work piece. The second action is in the dwell period during which the tool keeps on rotating at the plunge point. In this phase the material around the tool is heated due to the friction between the probe and matrix surfaces due to sliding action. Due to this thermo-mechanical action, materials around the tool get plasticized. The third phase of action is in the steady state welding period, during which the rotating tool is traversed along the welding line. This is followed by a second dwell period, which is the fourth phase of action. The last and the fifth phase of action is in the releasing period during which the rotating tool is raised up from the weld line leaving behind a pin cavity in the work piece.

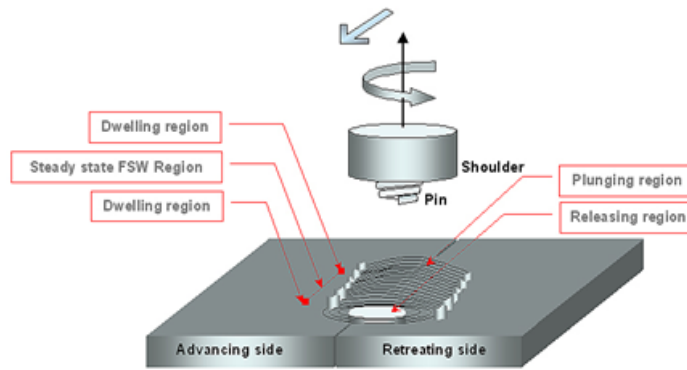


Fig. 1.3 Schematic of Friction Stir Welding

As for any welding process, there are a large number of process parameters that must be controlled in order to achieve a good welded joint. The parameters to be considered are as follows.

**Side clamping force** : The side clamping force, which holds the base material together, needs to be greater than the force generated by the stirring tool pin because the dimension of the tool pin increase at the same time. It has been observed that if the clamping force is not high enough, void is present, just below the surface on the advancing side of the weld.

**Length of tool pin** : To ensure sufficient plastic deformation in the root of the weld, the length of the pin should be related to the wall thickness. If the length of the pin is too short, a defect in the root can be generated and early fracture during tensile or root bend testing will occur. This type of defects can also act as crack initiation site as well as an easy path for crack propagation. On the other hand, if the tool pin length is excessive, the tool will contact the backing plate and suffer damage.

**Thickness** : When the thickness of the substrate, many process parameters as well as tool design have to be adjusted, due to change in heating and height of the weld. If the material is too thick or the tool too short a region of non-welded material would exist near the weld root, therefore, it is important with a consistent thickness.

**Tool geometry** : The tool geometry is an important parameter for FSW. Tool pin shape influences the heat generation, plastic flow and the stirring action in the weld. Moreover, the tool pin size is reflected in the width of the weld. The FSW shoulder and the pin geometry are adapted to the work material and its thickness. Microstructure changes can occur when the tool design is modified. The most common tool today has a threaded pin whereas the older ones had a more simple geometry. The shoulder should act as a heat pump to assist the softening of the material around the rotation pin. The most common shoulder has a flat underside. It has been observed that presence of voids is related to the welding speed. A rapid increase in the rotation speed can produce small voids. The mechanism behind this behavior is not known at present.

**Tool rotation speed** : The tool rotation speed used so far for Al 6061-T6 is between 500 and 1200rpm. The rotation speed must be large enough to generate sufficient heat to soften the Al alloy so that tool fracture will not occur. When the development of the process came to thicker sections of copper the rotation speed had to be increased to match the increased heat conduction away from the weld zone. The higher speed resulted in improved lifetime but a small triangular shaped void was sometime present near the top surface on the advancing side. Increasing the side clamping force and axial welding force could eliminate this void. The rotation speed is considered as a most significant process variable.

**Tilt angle** : Most FSW trials on Al alloys have had a tool tilt angle of 2–3°. The reason for exploring an increased tool tilt angle is to improve the forging of the back edge of the tool shoulder. In the way, it may be possible to eliminate sub-surface voids. In aluminum welds, an increase from 0° to 2° in tilt angle gives a dramatic change in the microstructure development and material flow. A larger tilt angle gives a tighter weld, and a more uniform material flow. When welding aluminum alloys it has been observed the major effect of the tilt angle is to press down the material on the trailing edge. This material flow results in flash on both the advancing and retreating sides. This flash



does not influence the weld integrity since it can be machined off from the surface.

### 1.3 Method of study

The numerical analysis program is developed by applying the theory of non-stationary heat conduction and thermal elasto-plasticity.

Also, thermal and mechanical behaviour is verified by carrying out the numerical simulation against the weldments. The detailed method of study is as illustrated below.

In experiments, 90 trials has been carried out to obtain optimum welding condition by Friction Stir Welding. Tilt angle, tool geometry, thickness, room temp. are fixed and the other parameters changed as shown in below table. Normally, thickness plate require more exact measurement and control so only one by one changing parameters was applied in this stage.

#### 1.3.1 Numerical Simulation

##### (1) Analysis of Welding heat

This paper develops the computer program for analyzing the non-stationary heat conduction considering the effect of welding heat source, and the numerical simulation is carried out for weldments and the mechanical properties are verified.

- 1) The equation of non-stationary heat conduction is adopted and the heat conduction in solid material is formulated by finite element method using Galerkin method, and the Iso-parametric element is used for analysis.
- 2) The material is isotropic and temperature dependence of specific heat, coefficient of heat transfer, thermal conduction and density are applied, because they are varied by temperature change.

- 3) Both the heat that transfers out to the air on the surface of weldments and the radiation of heat are considered.
- 4) The thermal characteristics by change of welding pass in welds are examined.

## (2) Analysis of welding residual stress

The computer program, capable of analyzing the welding residual stresses which are generated by thermal load, is developed. And the mechanical behaviour in welds are examined by analyzing the results, obtained from the numerical simulation against both weldments.

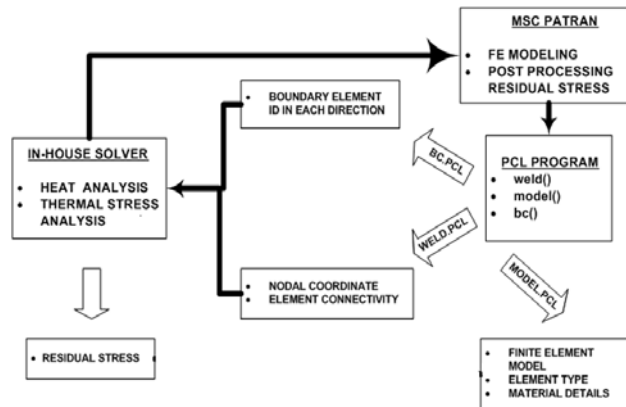


Fig. 1.4 Typical model of the data transferring

- 1) The temperature dependent mechanical properties such as yield strength and elastic modulus etc in elastic and plastic zone are considered.
- 2) In order to increase the accuracy of analysis, stress-strain and the stiffness matrix are derived by superposition.
- 3) The increment of total strain in elastic zone is obtained by the sum of elastic strain and thermal deformation. And the increment of strain in plastic zone is obtained by Plastic-flow theory, and Von-Mises yield conditions are used as yield function considering linear isotropic hardening law.

- 4) By using thermal elasto-plastic program, the numerical analysis for both dissimilar and similar weldments and the occurrence mechanism, magnitude and distribution pattern of welding residual stresses and of plastic strain are examined closely and mechanical characteristics are presented.

### 1.3.2 Experiment

Both dissimilar and similar weldments, identical with the specimens which are used for numerical analysis, are fabricated and the welding residual stresses are measured to compare with the results calculated with numerical analysis. And mechanical tests such as tensile, bending and hardness and the examination of micro-structures, SEM(Scanning Electron Microscopy), EDS(Energy Dispersive X-ray Spectroscopy) and OM(Optical Microscope) are performed in accordance with the national standard (KS)

- 1) Dissimilar weldments are fabricated and the welding residual stresses are measured with XRD(X-Ray Diffractometer). The property of the calculated residual stresses are proved by comparing it with the experimentally measured stresses.
- 2) With the mechanical tests (tensile, bending and hardness), carried out in accordance with the national standard (KS) and examination of micro-structures in welds (weld metal, HAZ and base metal), the welded joints are verified experimentally.
- 3) Through the examination, the differences of material depletion and of welding defects in both dissimilar and similar welds are verified.

## Chapter 2

# Thermal, elastic–plastic theory and mathematical model for heat input

In this chapter, elastic–plastic theory that normally known was formulated to be applied to numerical analysis.

## 2.1 Theory of Heat conduction and thermal elasto–plastic analysis

The spatial and temporal temperature distribution satisfies the following governing equation of un–stationary heat conduction:

$$\rho c \frac{\partial T}{\partial t} = \lambda \left( \frac{\partial^2 T}{\partial x^2} + \frac{\partial^2 T}{\partial y^2} + \frac{\partial^2 T}{\partial z^2} \right) + \dot{Q} \quad (2.1)$$

where  $T$  is temperature( $^{\circ}\text{C}$ ),  $\rho$  is density( $\text{g}/\text{cm}^3$ ),  $\dot{Q}$  is rate of temperature change due to heat generation per volume ( $\text{cal}/\text{cm}^3 \cdot \text{sec}$ ),  $t$  is time (sec),  $\lambda$  is thermal conductivity of isotropic material ( $\text{cal}/\text{cm} \cdot \text{sec} \cdot ^{\circ}\text{C}$ ) and  $c$  is specific heat ( $\text{cal}/\text{g} \cdot ^{\circ}\text{C}$ ).

Heat conduction problem for the object of analysis is formulated as the finite element method using Galerkin method.

Internal temperature of the element,  $T$ , is given by

$$T(x, y, z, t) = [N(x, y, z)] \{ \phi(t) \} \quad (2.2)$$

where  $[N]$  is a shape function matrix shown the relation between nodal temperature and internal temperature of the element.  $\{\phi\}$  is the vector of the nodal temperature of the element at time  $t$ .

If Galerkin method is applied in Equation (2.1) using  $[N]$  as a weighting function at this time, following equation is obtained.

$$\int_{V^e} [N]^T \left\{ \lambda \left( \frac{\partial^2 T}{\partial x^2} + \frac{\partial^2 T}{\partial y^2} + \frac{\partial^2 T}{\partial z^2} \right) + \dot{Q} - \rho c \frac{\partial T}{\partial t} \right\} dV = 0 \quad (2.3)$$

where superscript,  $T$ , shows transformation of matrix and subscript,  $V^e$ , shows the domain of element.

Un-stationary heat conduction problem can be expressed as following finite element expression for an element.

$$[k]\{\phi\} + [c] \left\{ \frac{\partial \phi}{\partial t} \right\} = \{f\} \quad (2.4)$$

where  $[k]$ ,  $[c]$  and  $\{f\}$  show the heat conductivity matrix of an element, the heat capacity matrix of an element and the heat flow vector of an element, respectively. They are expressed as follows:

$$[k] = \int_{V^e} \lambda \left( \frac{\partial [N]^T}{\partial x} \frac{\partial [N]}{\partial x} + \frac{\partial [N]^T}{\partial y} \frac{\partial [N]}{\partial y} + \frac{\partial [N]^T}{\partial z} \frac{\partial [N]}{\partial z} \right) dV \quad (2.5)$$

$$[c] = \int_{V^e} \rho c [N]^T [N] dV \quad (2.6)$$

$$\{f\} = \int_{V^e} \dot{Q} [N]^T dV - \int_{S^e} q [N]^T dS \quad (2.7)$$

Boundary conditions on the boundary  $S_2$  to  $S_4$  can be given to substitute  $q$  in second term of equation (2.7).

- When the heat flux,  $q_o$ , flows from the boundary  $S_2$  :

$$\int_{S_2^e} q [N]^T dS = \int_{S_2^e} q_o [N]^T dS \quad (2.8)$$

- When heat transfer is on the boundary  $S_3$  for convection:

$$\int_{S_3^e} q [N]^T dS = \int_{S_3^e} \alpha_c (T - T_c) [N]^T dS \quad (2.9)$$

If  $T$  in the equation(2.9) is substituted, the equation(2.10) becomes as bellows:

$$\int_{S_3^e} q [N]^T dS = \int_{S_3^e} \alpha_c [N]^T [N] dS \cdot \{\phi(t)\} - \int_{S_3^e} \alpha_c T_c [N]^T dS \quad (2.10)$$

- When heat radiation is on the boundary  $S_4$  :

$$\int_{S_4^e} q [N]^T dS = \int_{S_4^e} \alpha_r (T - T_r) [N]^T dS \quad (2.11)$$

If  $T$  in the equation(2.11) is substituted by the equation(2.2), The equation(2.12) becomes as bellows:

$$\int_{S_4^e} q[N]^T dS = \int_{S_4^e} \alpha_r [N]^T [N] dS \cdot \{\phi(t)\} - \int_{S_4^e} \alpha_r T_r [N]^T dS \quad (2.12)$$

$$\begin{aligned} [k] = & \int_{V^e} \lambda \left( \frac{\partial [N]^T}{\partial x} \frac{\partial [N]}{\partial x} + \frac{\partial [N]^T}{\partial y} \frac{\partial [N]}{\partial y} + \frac{\partial [N]^T}{\partial z} \frac{\partial [N]}{\partial z} \right) dV \\ & + \int_{S_3^e} \alpha_c [N]^T [N] dS + \int_{S_4^e} \alpha_r [N]^T [N] dS \end{aligned} \quad (2.13)$$

$$\begin{aligned} \{f\} = & \int_{V^e} \dot{Q} [N]^T dV - \int_{S_2^e} q_0 [N]^T dS \\ & + \int_{S_3^e} \alpha_c T_c [N]^T dS + \int_{S_4^e} \alpha_r T_r [N]^T dS \end{aligned} \quad (2.14)$$

Therefore, finite element formula of an element can be derived as a form of matrix equation including boundary conditions by using equation (2.6), (2.13) and (2.14).

Finite element formula for the whole object analyzed is constructed with assembled each matrix of elements and it can be expressed as follows:

$$[K]\{\Phi\} + [C]\left\{\frac{\partial \Phi}{\partial t}\right\} = \{F\} \quad (2.15)$$

where  $[\Phi]$ ,  $[K]$ ,  $[C]$  and  $\{F\}$  show the vector of the nodal temperature in the whole object, the heat conductivity matrix in the whole object, the heat capacity matrix in the whole object and the heat flow vector in the whole object, respectively. They are given as bellows.

$$[\Phi] = \sum_e \phi, \quad [K] = \sum_e k, \quad [C] = \sum_e c, \quad \{F\} = \sum_e f \quad (2.16)$$

## 2.2 Theory of thermal elasto-plastic analysis

In the thermal elastic problem, basic equations such as 1) Equilibrium equation, 2) Equation of strain-displacement relation and 3) Equation of stress-strain relation are needed to solve the problem. 1) Equilibrium equation can be replaced by principle of virtual work. These equations, 1) Principle of virtual work, 2) Equation of strain-displacement relation and 3) Equation of stress-strain relation are used in finite element method as the basic equations. Each equation is given in matrix form as follows:

$$\int_V \delta\{\epsilon\}^T \{\sigma\} dV - \int_V \delta\{U\}^T \{\bar{F}\} dV - \int_{S_\sigma} \delta\{U\}^T \{\bar{T}\} dS = 0 \quad (2.17)$$

where  $\{\sigma\}$  : stress vector,  $\{\epsilon\}$  : strain vector,  $\{U\}$  : displacement vector,  $\{\bar{F}\}$  : body force vector per unit volume,

$\{\bar{T}\}$  : surface force vector per unit area,  $V$  : volume of an object, and

$S_\sigma$  : area given mechanical boundary condition.

$$\{\epsilon\} = [A]\{U\} \quad (2.18)$$

where matrix  $[A]$  includes the differential operator.

$$\{\epsilon\} = \{\epsilon^e\} + \{\epsilon^T\} \quad (2.19)$$



where  $\{\boldsymbol{\varepsilon}\}$  :total strain vector,  $\{\boldsymbol{\varepsilon}^e\}$  :elastic strain vector and  $\{\boldsymbol{\varepsilon}^T\}$  :thermal strain vector.

$$\{\boldsymbol{\sigma}\} = [\mathbf{D}^e] \{\boldsymbol{\varepsilon}^e\} \quad (2.20)$$

where  $[\mathbf{D}^e]$  is elastic stress-strain matrix. From the equation (2.19) and (2.20), an equation of stress-strain relation is obtained as follows.

$$\{\boldsymbol{\sigma}\} = [\mathbf{D}^e] (\{\boldsymbol{\varepsilon}^e\} - \{\boldsymbol{\varepsilon}^T\}) \quad (2.21)$$

$$[\mathbf{k}]\{\mathbf{d}\} = \{\mathbf{f}_s\} + \{\mathbf{f}_v\} + \{\mathbf{f}_T\} \quad (2.22)$$

where  $[\mathbf{k}]$  :stiffness matrix of element,  $\{\mathbf{f}_s\}$  :nodal force vector due to surface force,  $\{\mathbf{f}_v\}$  :nodal force vector due to body force and  $\{\mathbf{f}_T\}$  :pseudo nodal force vector due to thermal strain. These are consisted as bellows.

$$[\mathbf{k}] = \int_{V^e} [\mathbf{B}]^T [\mathbf{D}^e] [\mathbf{B}] dV \{\mathbf{d}\} \quad (2.23)$$

$$\{\mathbf{f}_s\} = \int_{S_G^e} [\mathbf{N}]^T \{\bar{\mathbf{T}}\} dS \quad (2.24)$$

$$\{\mathbf{f}_v\} = \int_{V^e} [\mathbf{N}]^T \{\bar{\mathbf{F}}\} dV \quad (2.25)$$

$$\{\mathbf{f}_T\} = \int_{V^e} [\mathbf{B}]^T [\mathbf{D}^e] \{\boldsymbol{\varepsilon}^T\} dV \quad (2.26)$$

Equilibrium equation for the whole object, the total elements, is obtained to assemble the equation (2.22) for each element.

## 2.3 Mathematic model for heat input

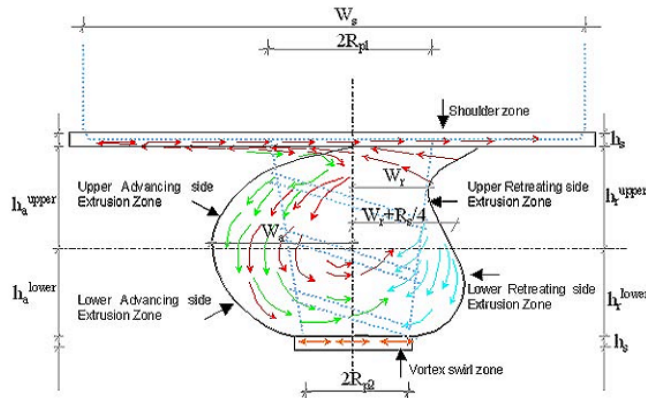


Fig. 2.1 Flow pattern model of FSW

Fig. 2.1 Schematics of metal flow pattern model of FSW and shape of the various sub zones in SZ

### Analytical model

In order to get the volume of heat input for Finite element analysis, the volume of the tool has been deducted from the total volume of the extrusion zone, shoulder zone and vortex swirl zone. The Advancing upper and lower extrusion zone and retreating lower extrusion zone has been defined using parabolic geometry and the Retreating upper extrusion zone by geometry as shown in Fig.2. The volume per unit time of the die cavity formation from Fig. 2.2 can be written as

$$V_{DC} = V_f (R_{p1} + R_{p2}) h t \quad (2.26)$$

$V^a$

where  $V^a$  – volume of the material moving through the Advancing side of extrusion zone

$$V^r$$

where –volume of the material moving through the Retreating side of extrusion zone

Volume of the material moving through the Retreating side of extrusion zone is given by

$$V^r = V_{\text{upper}}^r + V_{\text{lower}}^r - \text{die cavity.} \quad (2.27)$$

$$V_{\text{upper}}^r = (V_f - V_t) \left[ W_r + \frac{R_s}{24} + \lambda \delta^2 \right] h_r^u t. \quad (2.28)$$

$$V_{\text{lower}}^r = (V_f - V_t) \left[ \frac{2}{3} \left( W_r + \frac{R_s}{4} \right) + \lambda \delta^2 \right] h_r^l t. \quad (2.29)$$

Volume of the material moving through the Advancing side of extrusion zone is obtained as

$$V^a = (V_f + V_t) \left[ \frac{2}{3} W_a + \lambda \delta^2 \right] h t. \quad (2.30)$$

Assuming the material moved down one tread pitch (1/l) per revolution, total downward motion is obtained as

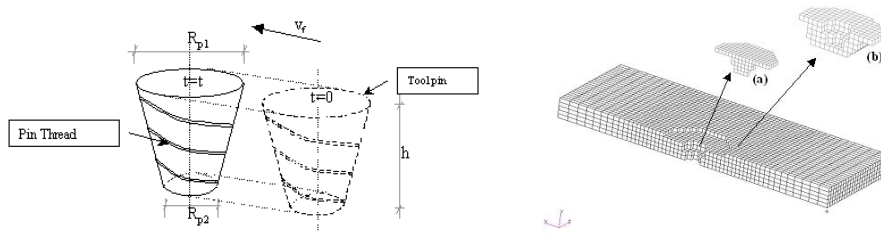
$$\Delta Z = \omega t / \lambda. \quad (2.31)$$

Total volume per unit time of the shoulder–processed material is given by

$$V_s = t \omega (R_s - R_p) * h_s / \lambda. \quad (2.32)$$

It is also assumed that the shoulder material fills the volume vacated by the downward motion. The plasticized metal is not allowed to expand freely due to the containment of its solid surrounding and the axial force from the tool. This result in the expulsion of metal at the top surface and the rotation of the tool transport this expelled metal and deposited them in the retreating side. In this work this volume is assumed as 2~4%  $V_s$  depending on the rotation speed. Equating the flow for mass balance will result the equation as

$$V_{DC} = V^e + 0.98V_s. \quad (2.33)$$



**Fig. 2.2 Shoulder, Extrusion, Vortex zone height and Width of Extrusion for various rotations and Translational speed of the tool**

By considering quadratic terms of general surface equation, we arrive at the nine-term bi-quadratic function:

$$h_i = a_{00} + a_{10}x + a_{01}y + a_{20}x^2 + a_{11}xy + a_{02}y^2 + a_{21}x^2y + a_{12}xy^2 + a_{22}x^2y^2 \quad (2.34)$$

Occasionally, the  $x^2y^2$  term is omitted,

So the equations for the height of shoulder vortex and extrusion zone from the above surface plots shown in Fig 5 are Based on the equation of the analytical model and bi-quadratic function of height of shoulder vortex extrusion zone and width of the stir zone an excel work sheet as shown in the Fig 2.3 has been created to calculate the dimension of the stir zone based

on the welding parameters.

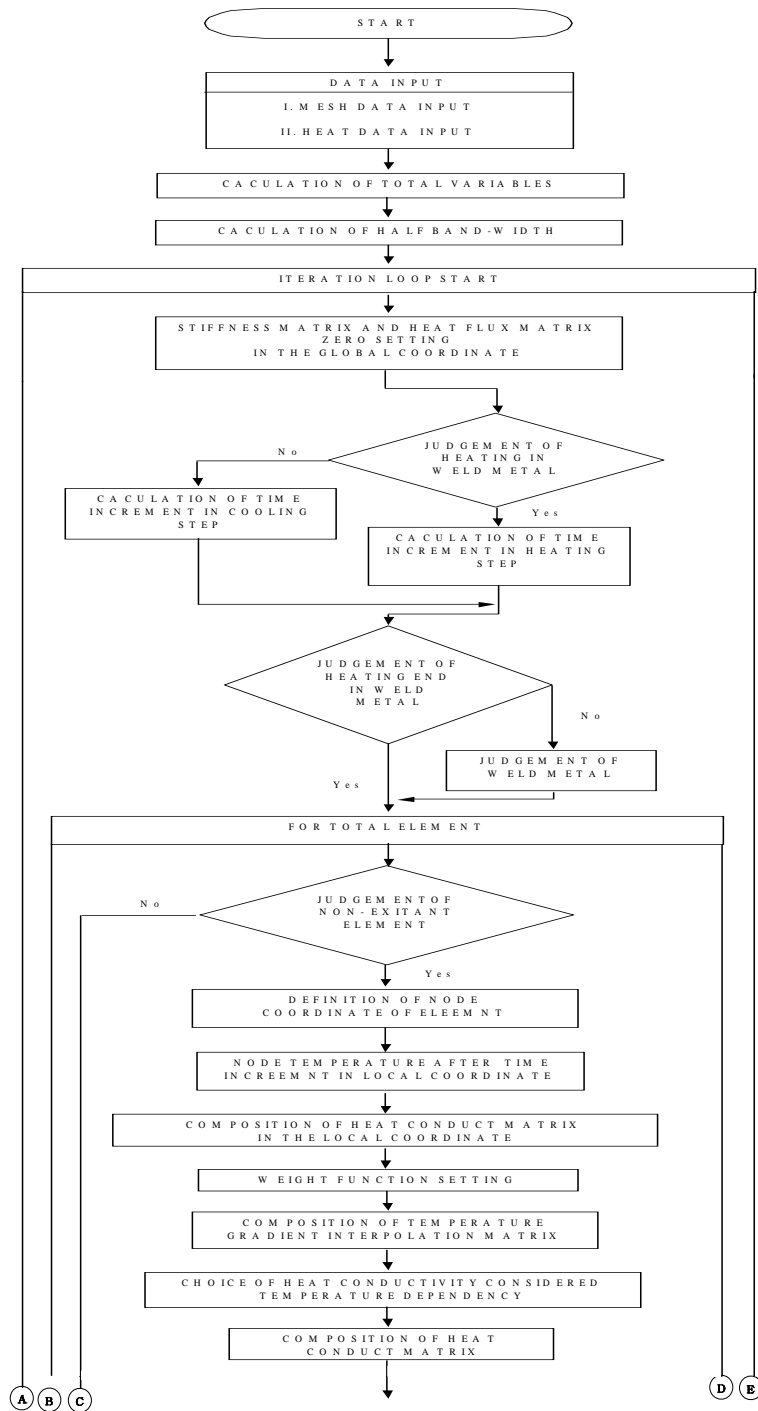
$I$	:	Threads per inch	$R_s$	:	Radius of shoulder
$d^2$	:	Projected thread area	$v_f$	:	Forward travel speed
$W_a$	:	Width of advancing extrusion zone	$v_t$	:	Pin tangential velocity = $2 R_{pw}$
$W_r$	:	Width of retreating extrusion zone	$v_s$	:	Velocity of material in shoulder zone
$W_s$	:	Average width of shoulder zone	$w$	:	Rotation speed
$DZ$	:	Distance material moves down per revolution	$h$	:	Pin length
$Q_{sa}, Q_{sr}$	:	Rate of heat generated	$h_s$	:	Depth of shoulder processing zone
$F_s$	:	Shear plane component of resultant force	$h_a$	:	Depth of advancing side extrusion zone
$R_{p1}, R_{p2}$	:	Radius of pin at top and bottom	$h_r$	:	Depth of retreating side extrusion zone

Variables	Values	units	Calculation Details
Rotational velocity= $w$	850	rpm	
Height of the pin= $h$	9	mm	
Top Radius of pin= $R_{p1}$	5.78	mm	
Bottom Radius of pin= $R_{p2}$	4.13	mm	
time = $t$	1	sec	
Radius of the shoulder= $R_s$	16	mm	
Projected area of the thread= $d \phi^2$	0.04	mm <sup>2</sup>	
Pitch of the thread= $\lambda$	1	Nos/mm	
Tangential velocity= $V_t$	140.673	mm/sec	
Translational Speed= $V_f$	4.5	mm/min	
Height of shoulder Zone=	0.963289675	mm	$(-5.65719 + 0.0294817^*w - 0.000023733^*w^2 - 0.0774083^*V_f + 0.0000265^*w^2V_f + 0.000581667^*V_f^2V_f)$
Height of Vortex Zone=	2.156671425	mm	$(16.9788 - 0.0382417^*w + 0.0000264667^*w^2 - 0.106575^*V_f + 0.0000435^*w^2V_f + 0.000741667^*V_f^2V_f)$
Height of Extrusion zone=	7.43916	mm	$(-9.79784 + 0.02542^*w - 0.000011^*w^2 + 0.31725^*V_f + 0.000177^*w^2V_f + 0.00194^*V_f^2V_f)$
Total width of extrusion Zone =	14.28014918	mm	$(24.6706 - 0.0154333^*w + 6.6666^*0.000001^*w^2 - 0.150667^*V_f + 0.00009^*w^2V_f + 0.000616667^*V_f^2V_f)$
Volume of the Die cavity= $V_{dc}$	670.275	mm <sup>3</sup>	
Volume of material moving through			
upper retreating extrusion zone $V_{r_{upper}}$	3843.567643	mm <sup>3</sup>	$495.355 W_r + 350.0509$
lower retreating extrusion zone $V_{r_{lower}}$	3649.957997	mm <sup>3</sup>	$330.237 W_r + 1320.947$
-Total retreating extrusion zone side=	7493.52564	mm <sup>3</sup>	$825.592 W_r + 1670.998$
-Total Advancing extrusion zone side=	15720.74688	mm <sup>3</sup>	$734.865 W_r + 10538.07$
-Total extrusion zone side $V_E$	22543.99752	mm <sup>3</sup>	$1560.46 W_r + 11538.8$
-Total Shoulder zone $V_g$	139.4682901	mm <sup>3</sup>	$V_{dc} = V_E + 0.98^*V_g$ Gives ---->> $W_r = 7.05255$
Width of the Retreating side =	7.052550717	mm	
Width of the Advancing side =	7.227598458	mm	

Fig. 2.3 Calculation for determination of the dimensions of the stir zone based on the Friction stir welding parameters

Thus the width of retreating and advancing side were calculated. Using this value the radial distance of the boundary of heat input volume from the axis of the tool has been determined in both advancing and retreating side and the radial distance at the leading side was interpolated from these values at various level (along the thickness direction). Thus the three dimensional analytical model of the heat input volume has been created and based on this the finite element heat transfer analysis has been carried out.

## 2.4 Flow chart of the FE analysis program



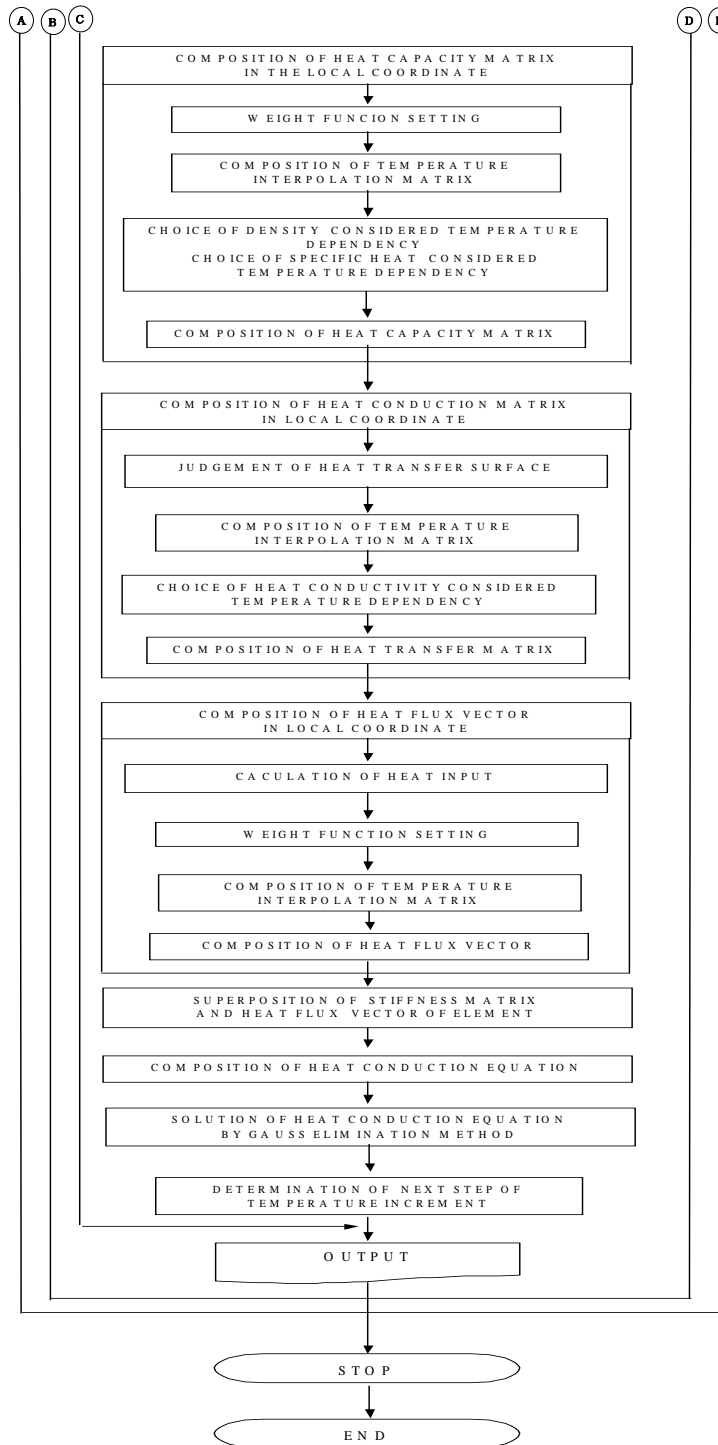
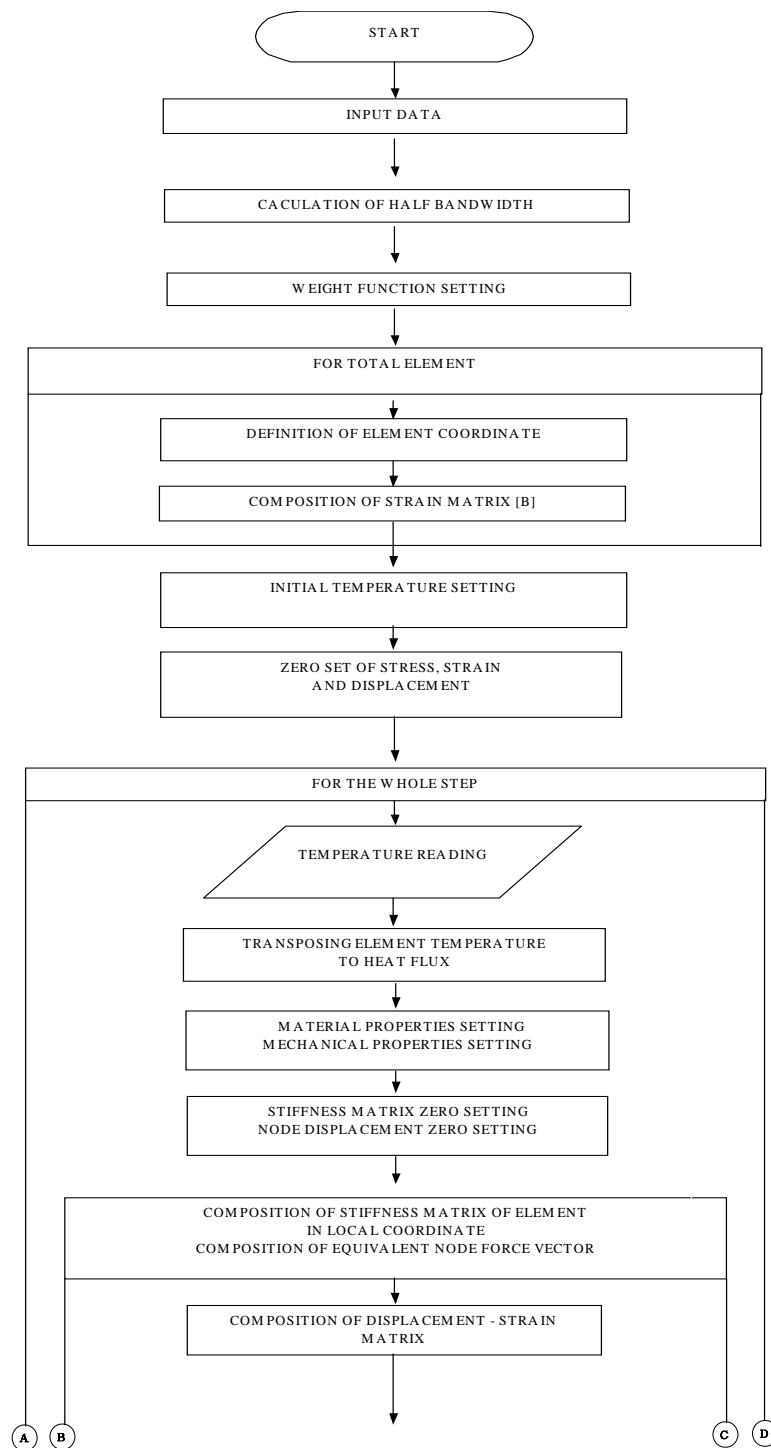


Fig. 2.4 Flow chart of the heat transfer analysis program





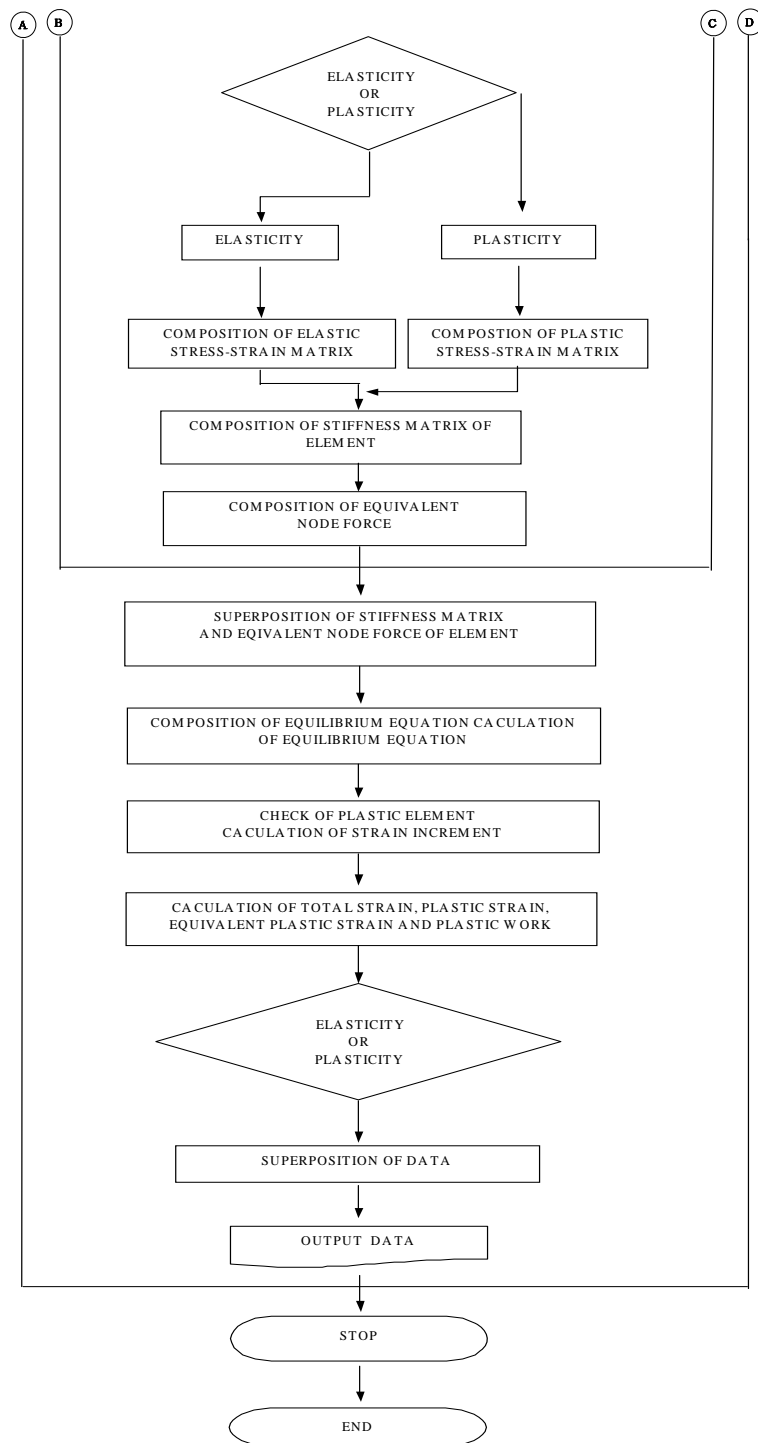


Fig. 2.5 Flow chart of the residual stress analysis program

## Chapter 3

### Numerical analysis of Friction Stir Welding

#### 3.1 Welding condition and Analysis model

Numerical analysis model was developed as per the weld geometry obtained from optimized welding condition.

##### 3.1.1 Analysis model(Al6061-T6 + AZ31)

As shown on Fig.3.1, The minimum dimension of similar (Al6061-T6 or AZ31) specimen ( $100 \times 200 \times 2t$ ) is selected to minimize the mechanical effect in welds such as contraction and expansion in weldment.

To analyse the temperature distribution and welding residual stresses in welded plate, the x-axis is placed in transverse direction of welding, the y-axis is placed along the thickness of the weldment, and the z-axis lies in the direction of welding.

Chemical compositions and mechanical properties are appeared on Table 3.1 and Table 3.2.

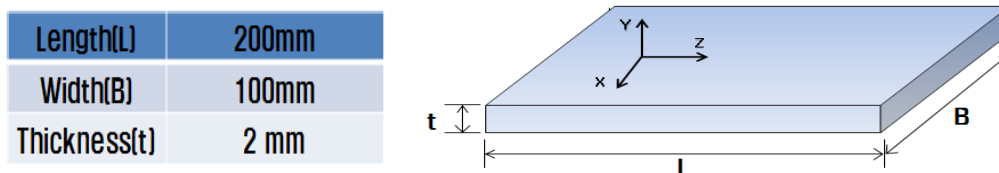


Fig. 3.1 Model for numerical analysis

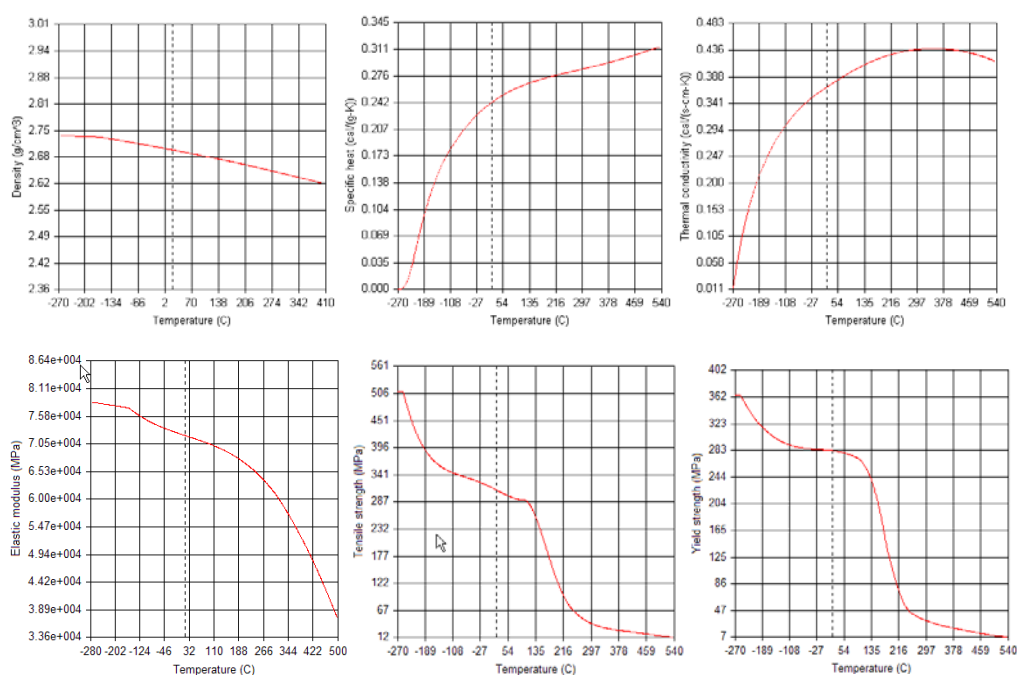
Table 3.1 Chemical compositions of Similar material

Base metal	Chemical compositions(%)							
	Al	Fe	Si	Cr	Mg	Cu	Mn	Zn
Al6061-T6	Bal.	0.7	0.4-0.8	0.04-0.35	0.8-1.2	0.15-0.4	0.15	0.25
AZ31	2.5-3.5	0.005	0.05	-	Bal.	0.05	0.2	0.7-1.3

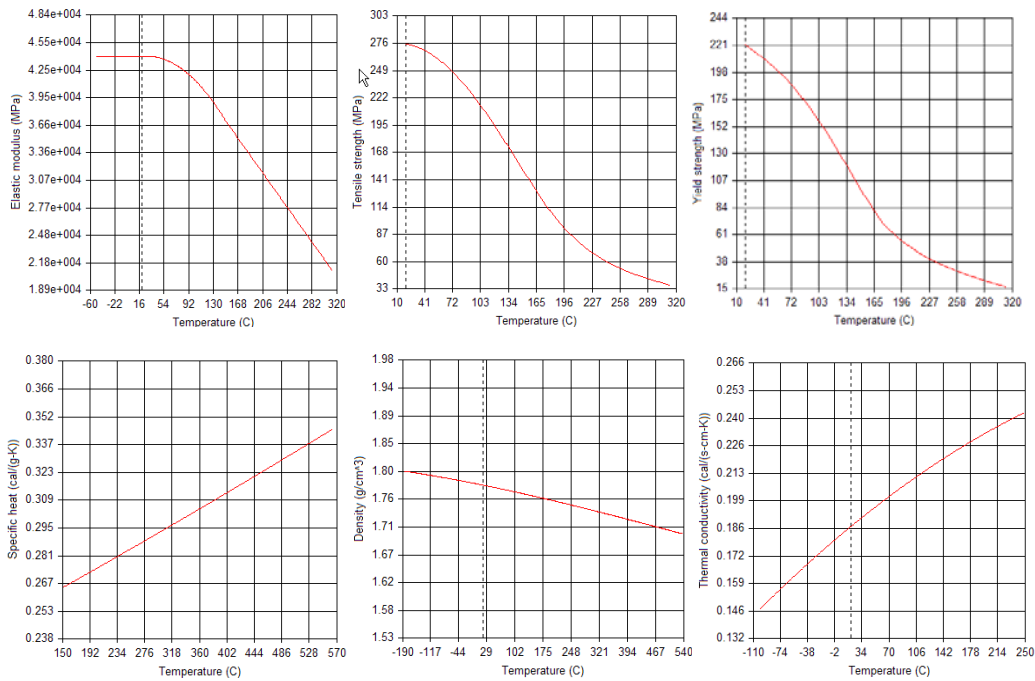
Table 3.2 Mechanical properties of Similar material

Base metal	Mechanical properties		
	Yield strength(Mpa)	Tensile stress(Mpa)	Elongation(%)
Al6061-T6	55	240	25
AZ31	220	290	15

Physical and temperature dependent mechanical properties of the material is illustrated in Fig3.2 .



#### 1) Temperature relativity of mechanical properties of Al6061-T6



2) Temperature relativity of mechanical properties of AZ31

Fig. 3.2 Temperature relativity of mechanical properties

FSW were performed at a rotation speed of 600 rpm and a welding speed of 0.3mm/sec, tool-to-work piece angle was maintained at approximately 1° and an effective plunge depth of 1.6mm. At these values of the welding parameters an adequate welding quality was obtained.

Table 3.3 Welding conditions

Rotation Speed(rpm)	Welding speed (mm/sec)	Shoulder size(mm)	Pin size (mm)	Room temperature
<b>600</b>	<b>0.3</b>	<b>12</b>	<b>4</b>	<b>20 °C</b>

Fig. 3.3 shows the element division of numerical analysis model of an FSW joint. The area which shows the large gradient of physical amount

(temperature, stress etc.) was fractionated more finely in consideration of heat distribution characteristics and stress variation characteristic.

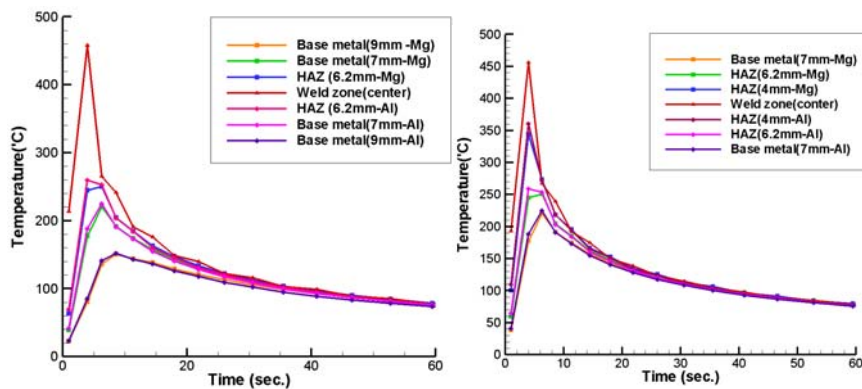
(Total element=1300, node=1441)



Fig. 3.3 Analysis Model and Mesh Division

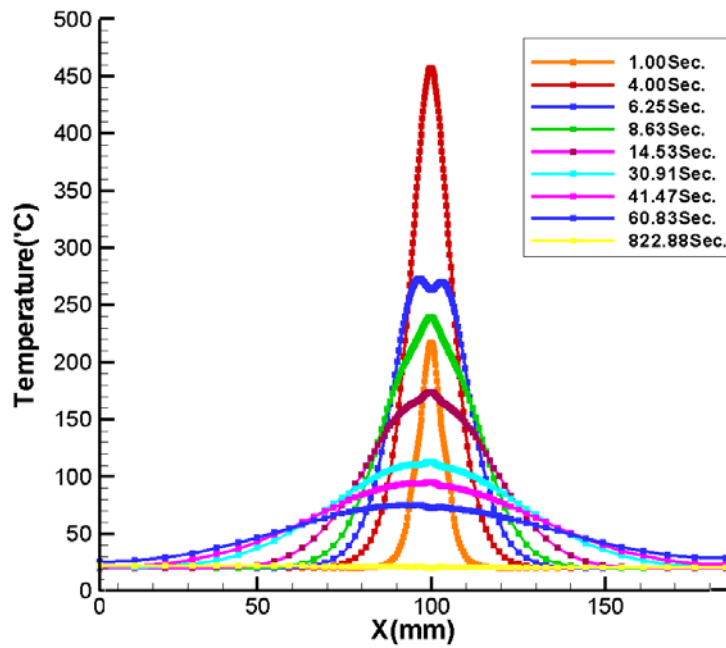
### 3.2 Temperature distribution

Fig. 3.4 shows thermal histories at different level of the FSW during joining. From the result shown, cooling time 450 °C to 270 °C of weld zone was calculated as about 4 sec. This graph shows that temperature going down abruptly. This is because analysis model was quite thin(2mm) and both of materials has high level of the thermal conductivity. Moreover, unstable temperature line was shown at 6.25sec, 30.91sec, 41.47sec and 60.83sec. Al6061-T6 and AZ31 has different conductivity and higher heat input than retreating side was concentrated in advancing side as well. However, those differences is slight and temperature values is going concordly, with increase in time.



1) 0.4mm below top surface

2) 1.6mm below top surface



3) Heat distribution of 0.2mm below top surface

Fig. 3.4 Heat distribution with respect to time

Fig 3.5 shows the isotherms of FSW. Heat affected zone were formed after 4 sec respectively from the start of heating, because same welding speed was adopted in all welding condition.

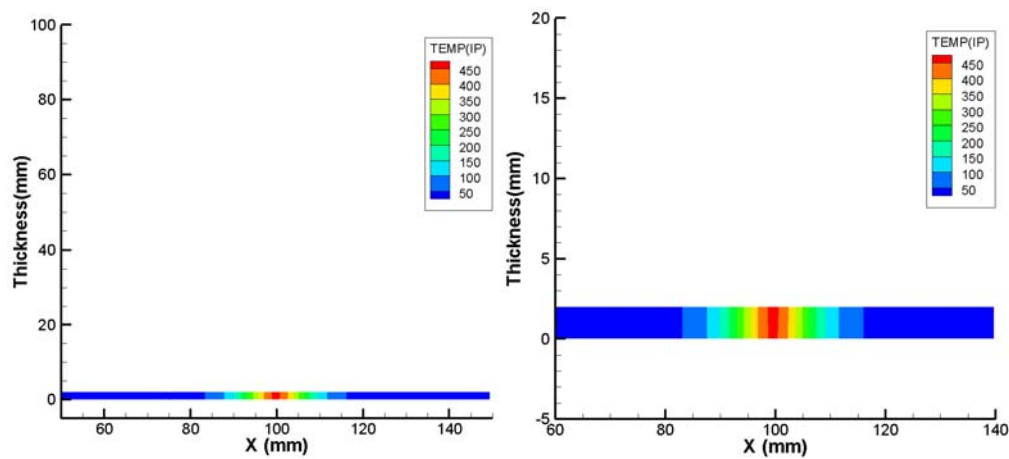


Fig. 3.5 Contour of heat distribution in FSW

### 3.3 Comparison of experimental and numerical results of residual stresses

The Fig. 3.6 shows residual stress distribution both measured(red) and analyzed(pink) values.

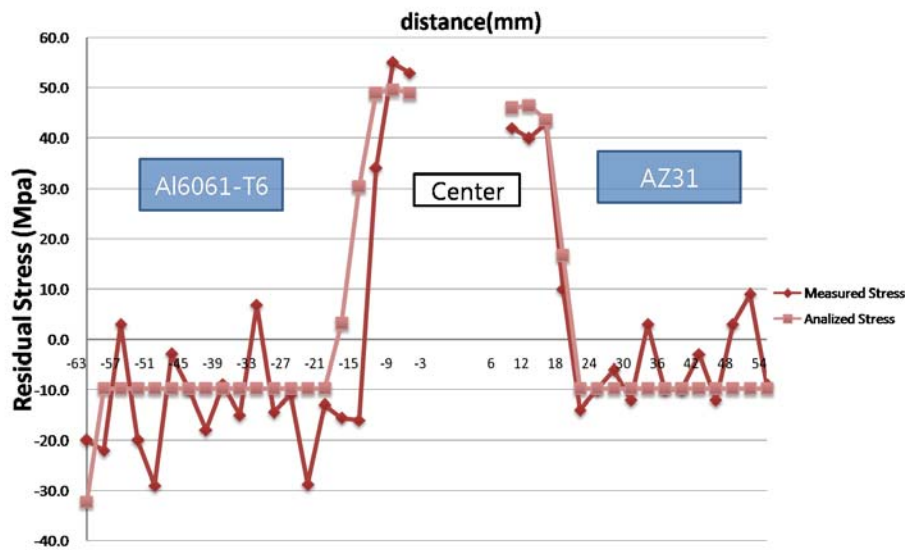


Fig. 3.6 Residual stress distribution

The welding residual stresses from numerical analysis and the measured welding stresses are seen distributed in similar pattern. It is revealed that the maximum stresses, measured in similar weldments, are generated similarly at both sides on center axis but the maximum stress is generated on the side of Al6061-T6. The analyzed residual stresses and the measured residual stresses are distributed in similar manner but the measured residual stresses is higher than the analyzed stresses.

## Chapter 4

### Experiment of Friction Stir Welding

Normally, Al alloy plate has used to be placed in retreating side because of its characteristics like less tough and rough, than AZ alloy. AZ alloy cannot cause sufficient plastic flow during FSW processing at weldment.

In this thesis, plate position of Al alloy is also significant parameter and compared to opposite condition.

#### 4.1 Friction Stir welding Machine and dimension of tool

Experiment was carried out by FSW which made by Winxen Co. Ltd., The capacity of equipment is shown on below table.



ITEMS		RANGE
TYPE		GENTRY TYPE
Welding Speed	X-axis	0.5~10 mm/sec
	Y-axis	0.5~10 mm/sec
	Z-axis	0.5~10 mm/sec
	R-axis	1~20 RPM
Rotation		300~3000 RPM
LOAD Capacity		Max. 3000Kgf

Fig. 4.1 FSW equipment and capacity

In this paper, shape of tool is same as shown in Fig.4.2 and design and the tool is made of KSD 3522 tool-steel tempered by HRC 64~65, having shoulder diameter of 12mm. The pin has height of 1.6mm, upper and lower



diameter of – and –mm respectively.

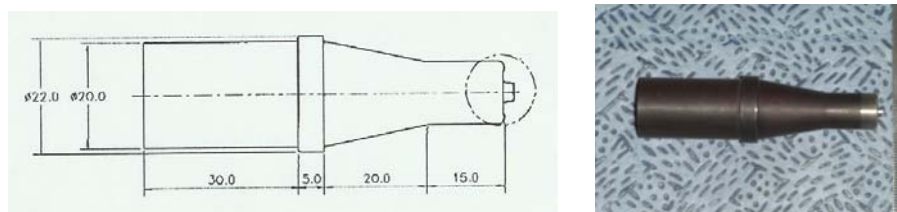


Fig. 4.2 Tool shape and drawing

Width of all specimen is 100mm and length is 200mm and thickness is 2mm. Bead On Plate trials were carried out in few specimens.

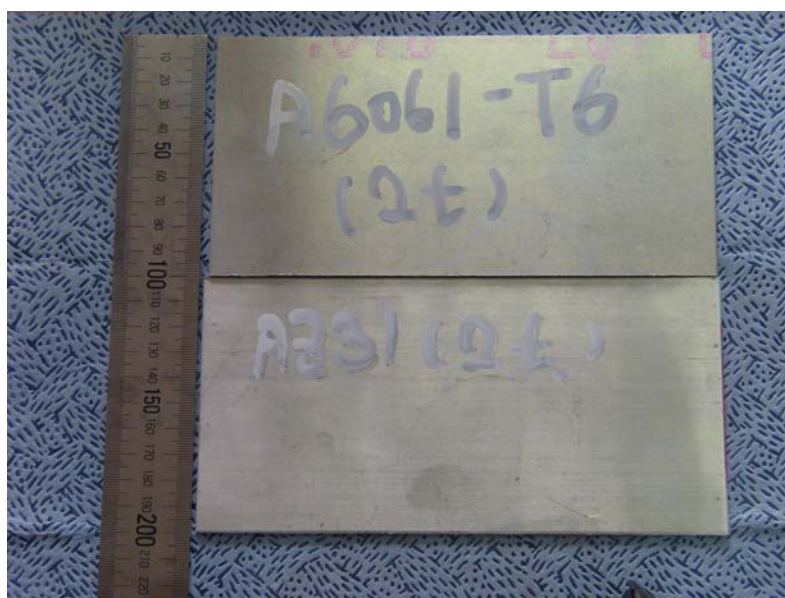


Fig. 4.3 Specimen size

## 4.2 welding conditions and bead shape

### 4.2.1 welding conditions

There are many parameters to be considered for FSW processing, but this thesis considered travel speed, RPM, penetration depth, tool input position and material position.

Range of RPM was limited from 1300 to 600 and tool penetrating point was 2mm away from edge of AZ31 specimen and penetration depth slightly changed according to temperature of FSW equipment because tool size and backing plate could be expanded after many times of welding trials.

Table 4.1 List of welding condition






NUMBER	MATERIAL	Adv. side	ANGLE	TRAVER SPEED	RPM	PIN	SHOULDER	TOOL INPUT POINT	PENETRATION DEPTH
1(X)	Al+Mg	Mg	1	3.3	1300	4mm	12mm	2mm	98.34
2	Al+Mg	Mg	1	5	1300	4mm	12mm	2mm	98.34
3	Al+Mg	Mg	1	6.6	1300	4mm	12mm	2mm	98.34
4	Al+Mg	Mg	1	8.3	1300	4mm	12mm	2mm	98.34
5	Al+Mg	Mg	1	10	1300	4mm	12mm	2mm	98.34
6	Al+Mg	Al	1	10	1300	4mm	12mm	2mm	98.34
7	Al+Mg	Al	1	10	1300	4mm	12mm	2mm	98.34
8	Al+Mg	Al	1	8.3	1300	4mm	12mm	2mm	98.34
9(X)	Al+Mg	Al	1		1300	4mm	12mm	2mm	98.34
10	Al+Mg	Al	1	5	1300	4mm	12mm	2mm	98.34
11	Al+Mg	Al	1	3.3	1300	4mm	12mm	2mm	98.34
12	Al+Mg	Al	1	1.6	1300	4mm	12mm	2mm	98.34
13	Al+Mg	Al	1	5	1300	4mm	12mm	2mm	98.34
14	Al+Mg	Al	1	5	800	4mm	12mm	2mm	98.34
15	Al+Mg	Al	1	0.3	400	4mm	12mm	2mm	98.34
16	Al+Mg	Al	1	1.6	450	4mm	12mm	2mm	98.54
17	Al+Mg	Al	1	1.6	500	4mm	12mm	2mm	98.54
18	Al+Mg	Al	1	3.3	500	4mm	12mm	2mm	98.54
19	Al+Mg	Al	1	5	500	4mm	12mm	2mm	98.54
20	Al+Mg	Al	1	6.6	500	4mm	12mm	2mm	98.54
21	Al+Mg	Al	1	6.6	600	4mm	12mm	2mm	98.64
22	Al+Mg	Al	1	6.6	1000	4mm	12mm	2mm	98.64
23	Al+Mg	Al	1	6.6	1000	4mm	12mm	center	98.64




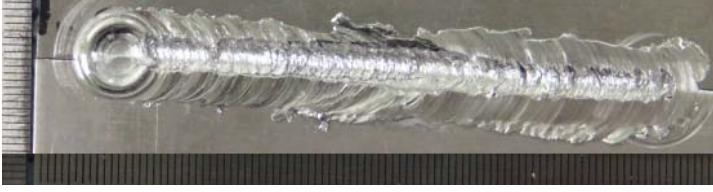




24	Al+Mg	Al	1	5	1000	4mm	12mm	center	98.64
25	Al+Mg	Al	1	5	1000	6mm	24mm	center	98.64
26	Al+Mg	Al	1	1.6	1000	4mm	12mm	center	98.64
27	Al+Mg	Al	1	3.3	1000	4mm	12mm	center	98.64
28	Al+Mg	Al	1	3.3	1200	4mm	12mm	center	98.64
29	Al+Mg	Al	1	1.6	1200	4mm	12mm	2mm	98.7
30	Al+Mg	Al	1	1	1200	4mm	12mm	2mm	98.74
31	BOP	Al	1	1	800	4mm	12mm	2mm	98.76
32	BOP	Al	1	1	800	4mm	12mm	2mm	98.78
33	BOP	Al	1	1	800	4mm	12mm	2mm	99
34	Al+Mg	Al	1	1	800	4mm	12mm	2mm	99
35	Al+Mg	Al	1	0.8	800	4mm	12mm	2mm	99.1
36	Al+Mg	Al	1	0.7	800	4mm	12mm	2mm	99.1
37	Al+Mg	Al	1	0.8	800	4mm	12mm	center	99.1
38	Al+Mg	Al	1	1	800	4mm	12mm	2mm	99.1
39	Al+Mg	Al	1	0.6	800	4mm	12mm	2mm	99.1
40	Al+Mg	Al	1	0.8	900	4mm	12mm	2mm	99.1
50	Al+Mg	Al	1	0.8	1000	4mm	12mm	2mm	99.1
51	Al+Mg	Al	1	0.8	700	4mm	12mm	2mm	99.1
52	Al+Mg	Al	1	0.8	600	4mm	12mm	center	99.1
53	Al+Mg	Al	1	0.8	500	4mm	12mm	center	99.1
54	Al+Mg	Al	1	0.8	550	4mm	12mm	center	99.1
55	Al+Mg	Al	1	0.8	650	4mm	12mm	center	99.1
56	Al+Mg	Al	1	1	600	4mm	12mm	center	99.1
57	Al+Mg	Al	1	0.6	600	4mm	12mm	center	99.1
58	Al+Mg	Al	1	0.4	600	4mm	12mm	center	99.1
59	Al+Mg	Al	1	0.3	600	4mm	12mm	center	99.1
60	Al+Mg	Al	1	0.15	600	4mm	12mm	center	99.1
61	Al+Mg	Al	1	0.3	700	4mm	12mm	center	99.1
62	Al+Mg	Al	1	0.3	600	4mm	12mm	2mm	99.1
63(x)	Al+Mg	Al	1	0.3	600	4mm	12mm	2mm	99.1
64(X)	Al+Mg	Al	1	0.3	600	4mm	12mm	2mm	99.1
65—1	Al+Mg	Al	1	0.3	600	4mm	12mm	center	99.1
65—2	Al+Mg	Al	1	0.3	600	4mm	12mm	center	99.1
66—1	Al+Mg	Al	1	0.3	600	4mm	12mm	center	99.1
66—2	Al+Mg	Al	1	0.3	600	4mm	12mm	center	99.1
67	Al+Al	small	1	0.3	600	4mm	12mm	center	99.1
68	Mg+Mg	small	1	0.3	600	4mm	12mm	center	99.1
69	Al+Al	big	1	0.3	600	4mm	12mm	center	99.1
70	Mg+Mg	big	1	0.3	600	4mm	12mm	center	99.1

## 4.2.2 Bead shape




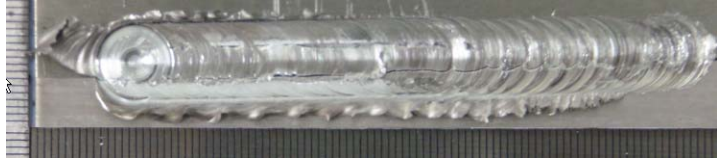




Table 4.1 shows different trials of FSW to get the optimum condition and each bead shape were shown in below images.






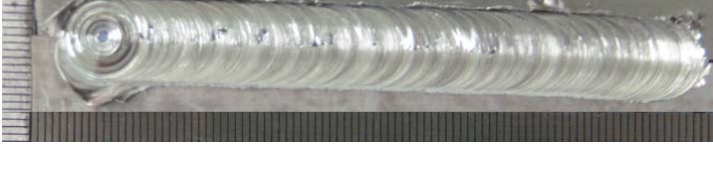

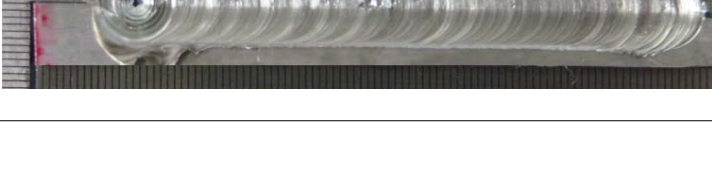
Table 4.2 Top bead shape


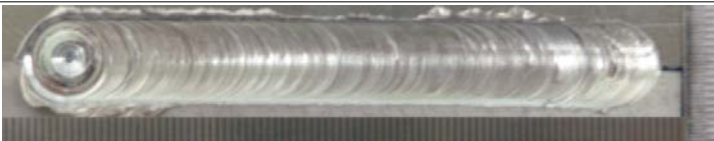

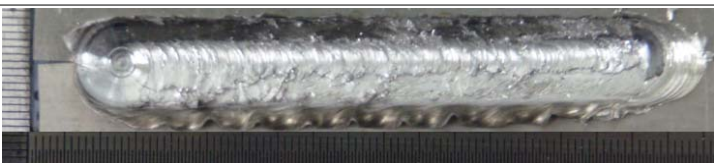




Number	Shape of top bead	Remark
17		BAD
18		BAD
19		BAD
20		BAD
21		BAD

22		BAD
23		BAD
24		BAD
25		BAD
26		BAD
27		BAD
28		BAD
29		BAD




30		BAD
34		BAD
35		BAD
36		BAD
37		BAD
38		BAD
39		BAD
40		BAD

50		BAD
51		BAD
52		GOOD
53		BAD
54		NOT BAD
55		BAD
56		BAD
57		BAD

58		NOT BAD
59		GOOD
60		BAD
61		BAD
62		GOOD
66		GOOD
Al-Al Big size		GOOD
AZ-AZ Big size		NOT BAD



Al-Al small size		GOOD
AZ-AZ small size		GOOD

### 4.3 Experiment of stress measurement and mechanical properties of dissimilar welding

This chapter proves the propriety of results through comparing and examining the obtained results from numerical analysis with the welding residual stresses that are measured at the welded structure. Besides, the characteristic of residual stress distribution is measured experimentally and the adequate examination is carried out to see whether the welding defects exist or not

#### 4.3.1 Welding residual stress

The welding residual stress in dissimilar weldments (Al6061-T6 / AZ31) is measured by XRD which provide reliable quantitative data. XRD equipment use the X-ray source and it can automatically calculate values of residual stress. To obtain exact data of specimen, exposing time increased to 30 second (normally 10 second) and every 3mm point which is transverse direction with weld line was measured by XRD.

Also, the specimen for welding residual stresses is fabricated with the same conditions for numerical analysis, and then residual stresses are measured. The measured result is compared and analyzed with numerical analysis result.

## 1) Specimen

Specimens are fabricated on the same condition that is considered for numerical analysis, ie, the size of specimen, shown on Fig.3.1 and welding condition, listed on Table 4.3. And specimens for measurement and stress measurement appliances are shown in Fig. 4.5 and Fig. 4.6 respectively. The checkpoints for welding residual stresses are selected in accordance with the result of numerical analysis and measurement that is carried out at the centre along the width direction of weldments as shown on Fig.4.6.

In order to measure the welding residual stresses,

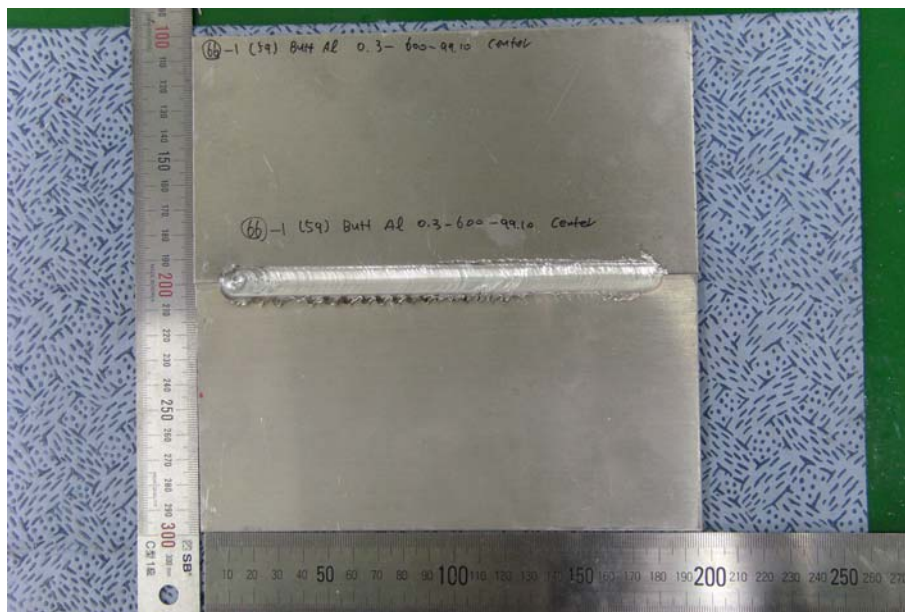


Fig. 4.4 Photograph of residual stress test specimens



Fig. 4.5 Residual stress measurement machine(XRD)

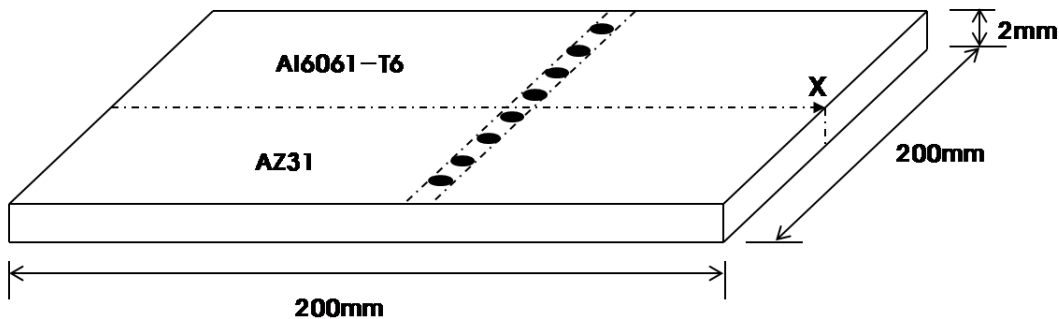


Fig. 4.6 Measurement Points of Welding Residual Stress

## 2) Welding residual stress measurement

The measured residual stresses of dissimilar weldments (Al6061-T6 + AZ31) are compared with the results of numerical analysis and examined closely.

### – Results of measurements of welding specimen

Considering the measured welding residual stresses of dissimilar specimen,

(Fig.4.4) the welding residual stresses is measured along the width direction of weldments. However, it shows us that the maximum stresses, measured near weldments, are generated similarly at both sides on center axis but the maximum stress is generated on the side of Al6061-T6. It is because of the difference of heat conductivity.

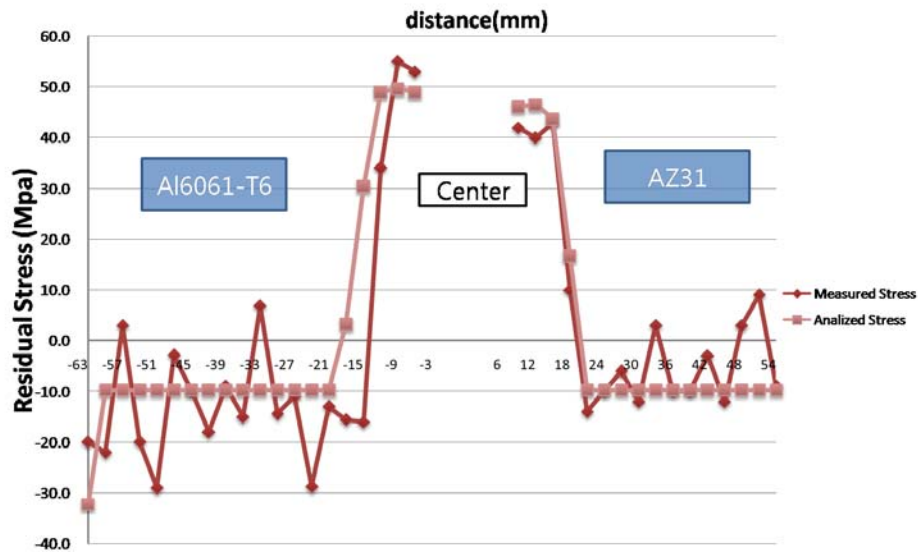


Fig. 4.7 Measurement results of welding residual stress

#### 4.4 Welding part mechanical property and micro-structure examination

This chapter carries out the mechanical tests such as tensile test, bending and micro-structure examination by using EDS and SEM. For these tests and examination, the specimens are machined in accordance with the national standards (KS). By the tests and examination, mentioned above, it is intended to establish the mechanical phenomenon of welded joint experimentally.

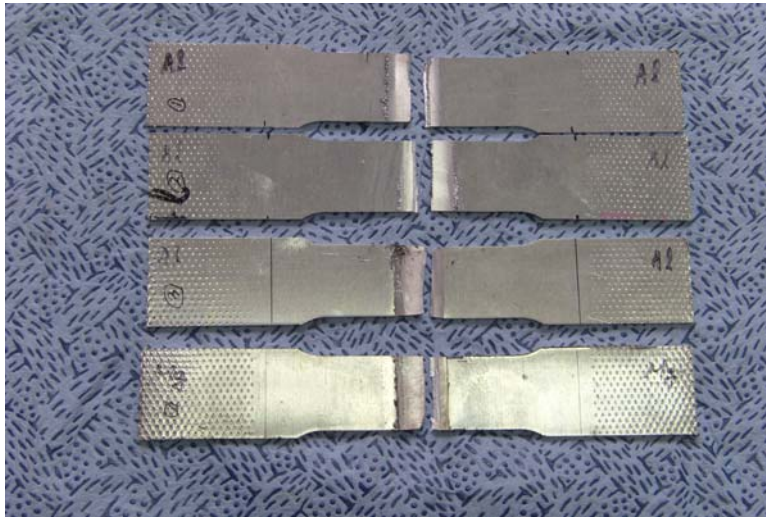
#### 4.4.1 Tension and a hardness test

In case of dissimilar weldments, 7 specimens for tensile are machined respectively and 3 specimens are machined for hardness test as well. Besides, in case of similar weldments, 8 specimens for tensile are machined respectively.

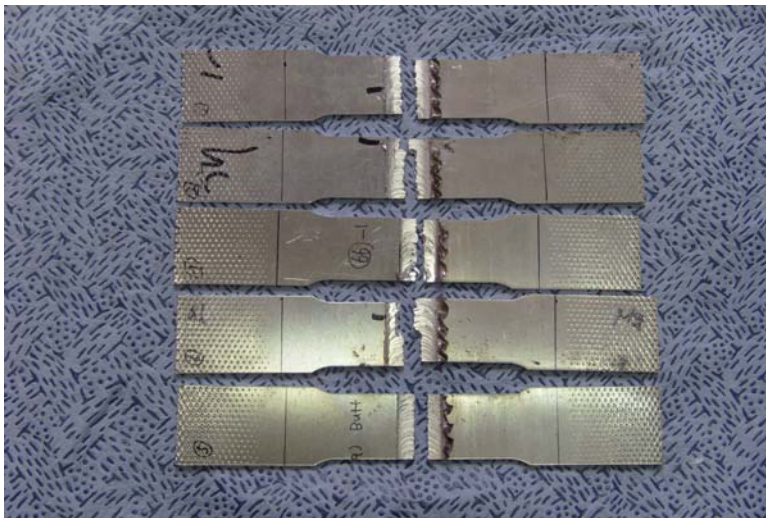
Tensile test is carried out with Universal Testing Machine (maximum load 50ton) of Dongil-Simaz Company. And Vickers Hardness Test Machine is used for hardness test. The specimens are fabricated in accordance with the national standards (KS0801-2)

##### 1) Result of Tension test

Table 4.3 shows the strength characteristic of both similar weldments (Al6061-T6 or AZ31) and dissimilar weldments (Al6061-T6 + AZ31) that are obtained by tensile test. As shown on pictures, the fracture occurred at weld zone in all specimens. Tensile strength of similar weldment agrees with that of weldments. The weld metal transforms very slightly until the specimens fractured, HAZ in vicinity of fractured area transformed relatively largely but HAZ, opposite of fractured area, did not transformed much. And the strength of dissimilar weldment is lower than that of similar weldment. Foremost, in the case of dissimilar joining that Al6061-T6 was placed at advancing side(this thesis),tensile strength is higher than adverse case that AZ31 was placed at advancing side. Normally, strength of weldment has been noticed that kinds of Al materials should be located at retreating side because of different ductility. however, this thesis shows that opposit case also could be available.



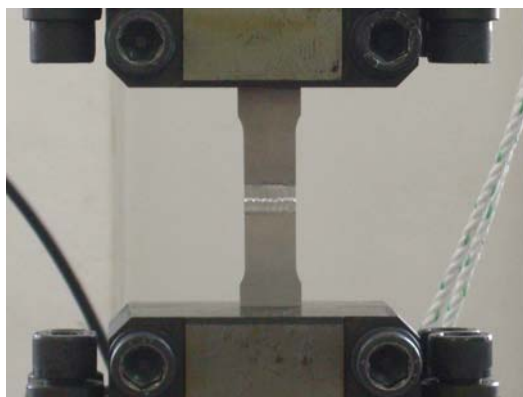
a) Tensile test specimen(similar welded joint)



b) Tensile test specimen(dissimilar welded joint)

Fig. 4.8 Photograph of tensile test specimen of similar & dissimilar welded joint





**G** – Gage length :  $25.0 \pm 0.08\text{mm}$   
**W** – Width :  $6.25 \pm 0.05\text{mm}$   
**T** – Thickness : 6mm  
**R** – Radius of fillet, min : 6mm  
**L** – Over-all length, min : 100mm  
**A** – length of reduced section, min : 32mm  
**B** – Length of grip section, min : 32mm  
**C** – Width of grip section, approximate : 10mm

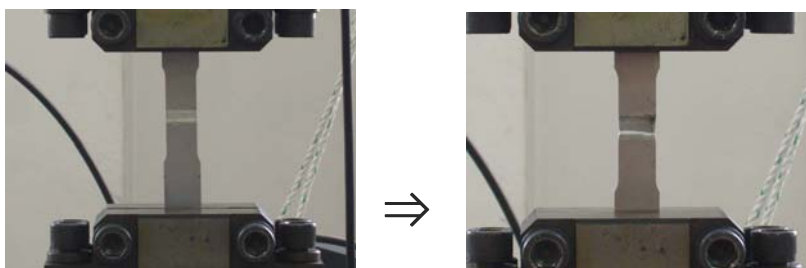
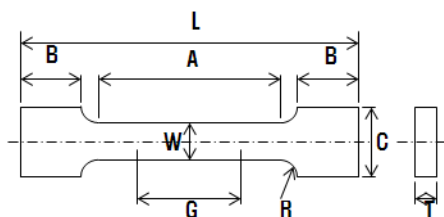
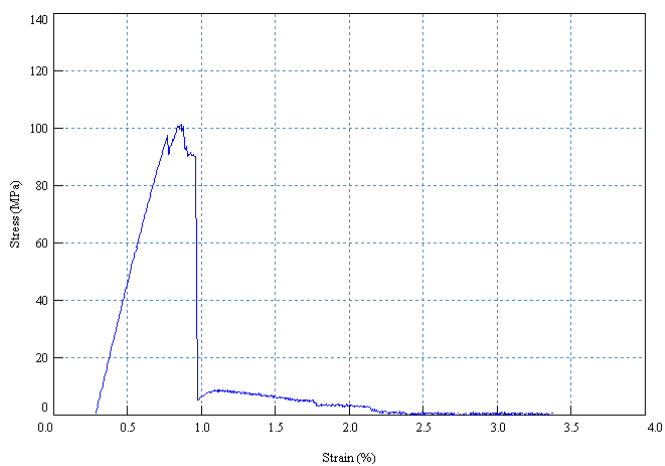
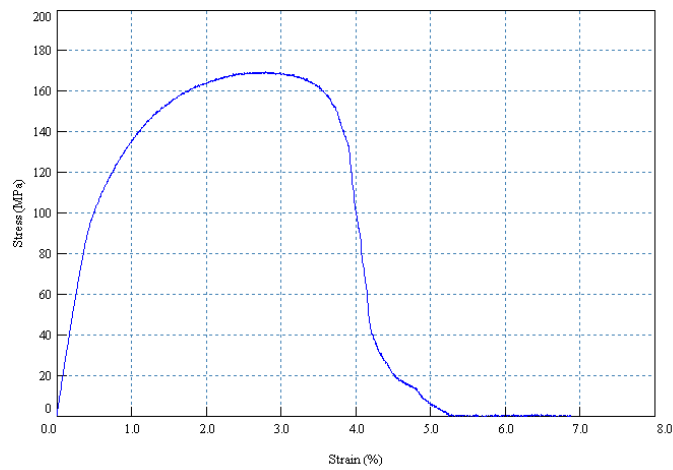


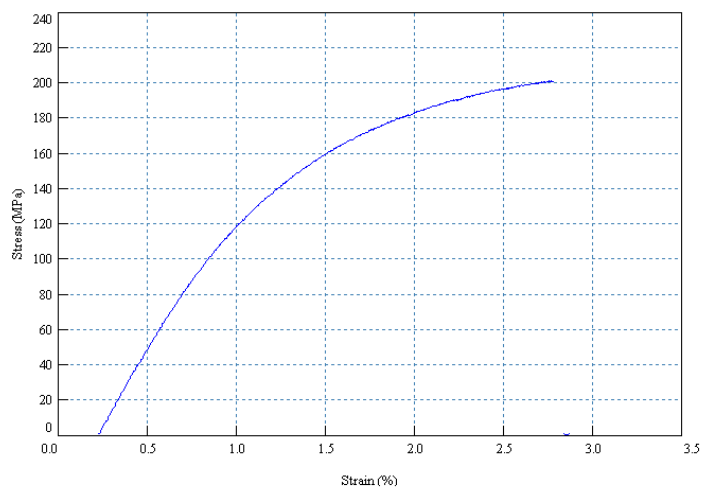
Fig. 4.9 Analysis model and mesh division



a) Dissimilar welded joint(Al6061-T6+AZ31)



b) Similar welded joint(Al6061-T6)



c) Similar welded joint(AZ31)

Fig. 4.10 Strain-stress graph of tensile test



Table 4.3 Result of tensile test

Specimen		Yield Strength (MPa)	Tensile Strength (MPa)	
Similar	1-1 (Al-Al)	92	150	
	1-2 (Al-Al)	68	75	
	1-3 (Al-Al)	95	170	
	1-4 (Mg-Mg)	67	200	
Dissimilar	2-1	98	102	
	2-2	69	69	
	2-3	94	110	
	2-4	90	115	
	2-5	93	110	

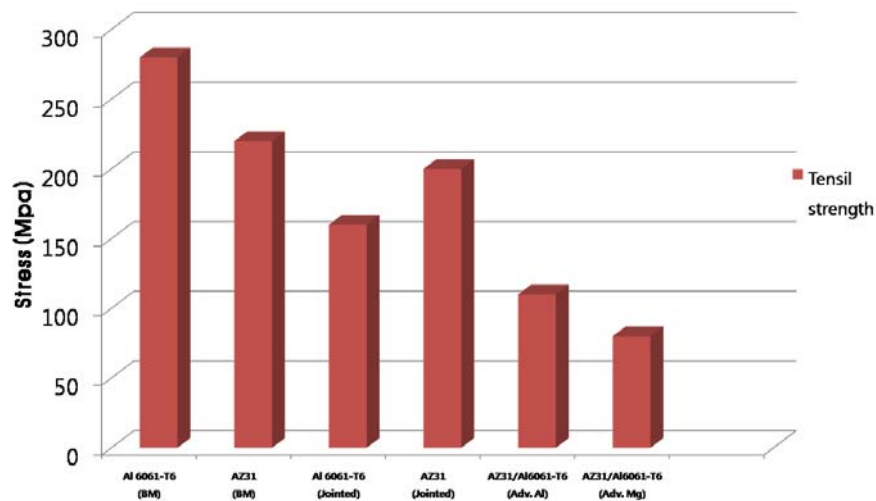


Fig 4.11 Result graph of tensile test

## 2) Hardness test result

Hardness test is carried out with Vickers Hardness Test Machine, shown on Fig. 4.12, and by load 0.5kgf. Fig. 4.13 shows specimens for hardness test. The hardness is measured at points 0.5mm below top surface. Fig.4.14 shows

the hardness distribution of dissimilar weldment. While the maximum hardness of dissimilar weldment appears in base metal, HAZ and weld metal of dissimilar weldment have lower value among that.

When comparing the hardness values of three weldments, the maximum hardness value of dissimilar weldment appeared on #52 that shown good top bead shape. The reason why hardness value of weldment appears lower than that of base metal in dissimilar welding joint is effect of different characteristics each other and weldment grain size shows uneven state. And the hardness value of dissimilar welding joint appears high in base metal because of the effect of phase.

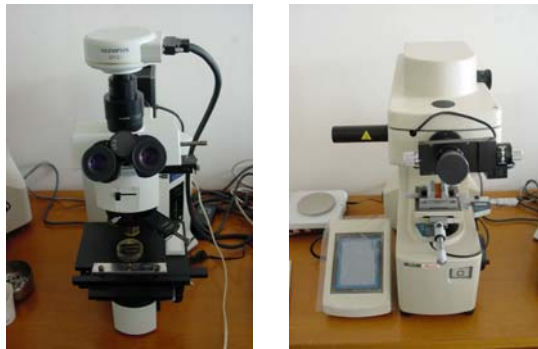


Fig. 4.12 Photograph of vickers hardness test machine

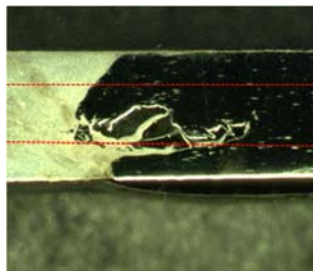
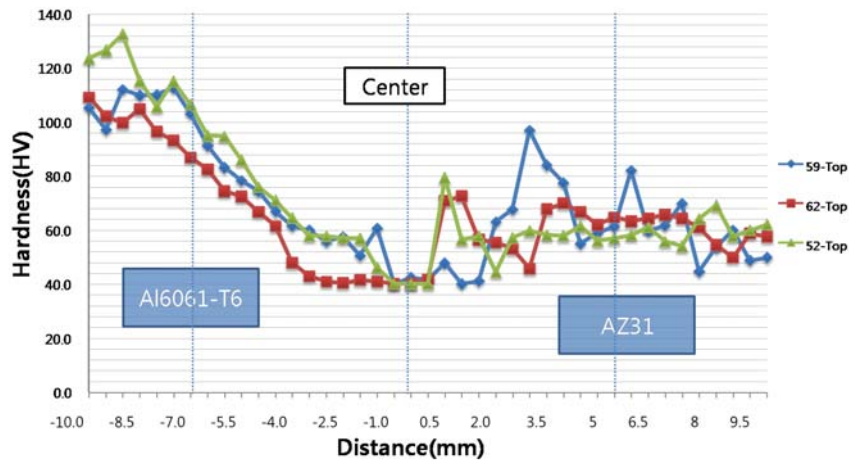
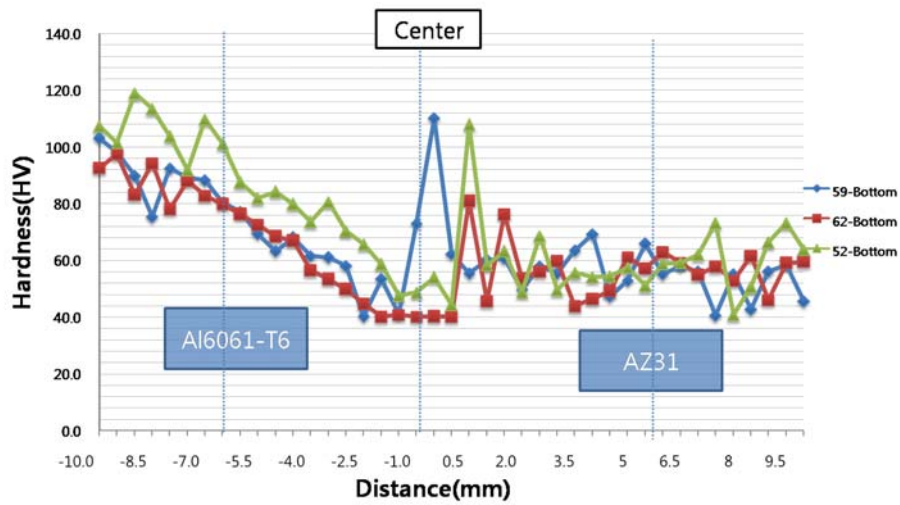


Fig. 4.13 Measurement points of hardness test (HV)



a) Result of hardness test specimen of dissimilar  
(0.5mm below top surface)



b) Result of hardness test specimen of dissimilar  
(1.5mm below top surface)

Fig. 4.14 Result of Hardness Test Specimen of Dissimilar Welded Joint

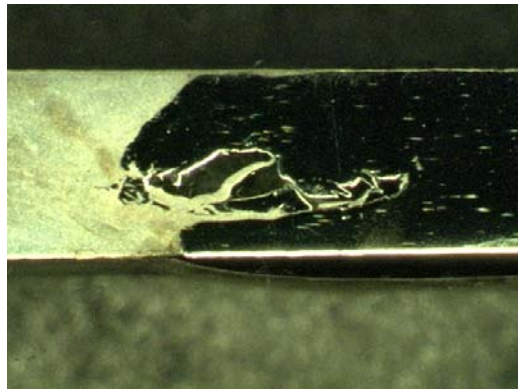
#### 4.4.2 Micro-structure examination by using Optical Microscope

The micro-structures for weld metal, HAZ and base metal are pictured and examined to figure out the change of micro-structure in similar weldment (Al6061-T6/AZ31) and in dissimilar weldment (Al6061-T6 + AZ31).

Similar and dissimilar welding specimens are fabricated to examine micro-structure picture as shown in Fig. 4.15.



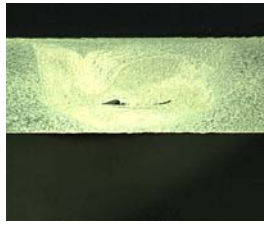
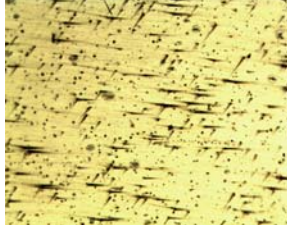

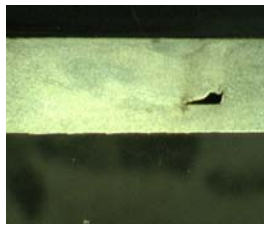
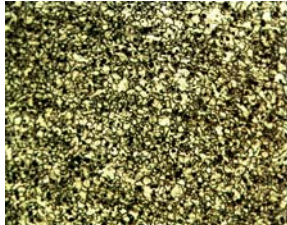
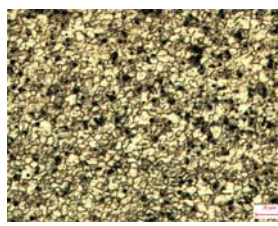


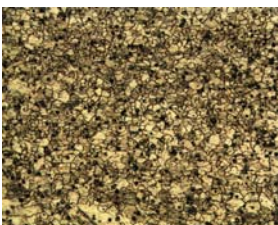
a) Cross section of similar welded specimen



b) Cross section of dissimilar welded specimen

Fig. 4.15 Photograph of macro-structure of similar & dissimilar welded specimen

Table 4.4 Cross section of welded joints

Specimen	Cross section	Weldment	Base metal
Similar Welding (Al6061-T6)			
Similar Welding (AZ31)			
Dissimilar Welding (Al6061-T6 + AZ31)			

#### 4.4.3 Micro-structure examination by using SEM and EDS

Below photos by SEM(Scanning Electron Microscopy), EDS(Energy Dispersive X-ray Spectroscopy) was prepared in order to analyzed in-depth phenomenon of FSW joining. Two welding condition, specimen number #52 and #59, shows good top bead shape and cross section also is same as well. SEM and EDS photo shows that boundary of each material was jointed well and ingredient ratio of Al6061-T6 and AZ31 also shows balanced value.

Table 4.5 Micro-structure observation of condition number 52


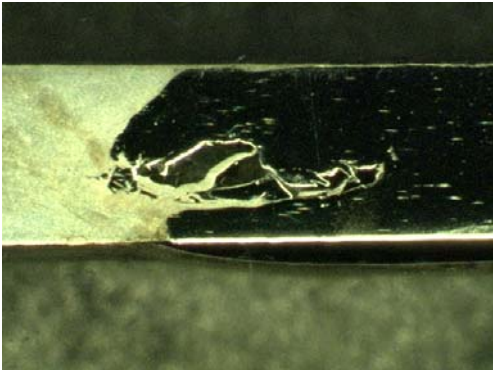
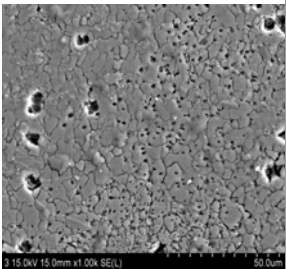
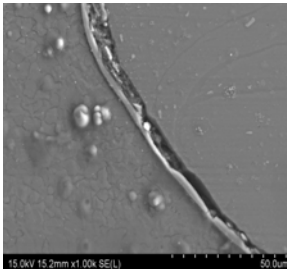
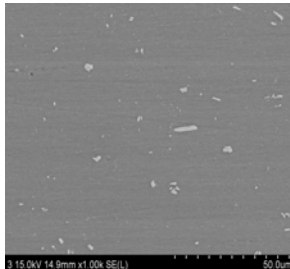
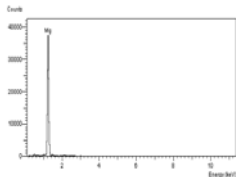
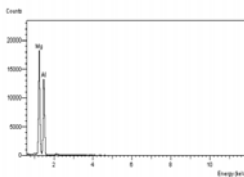
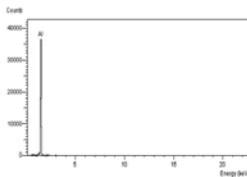
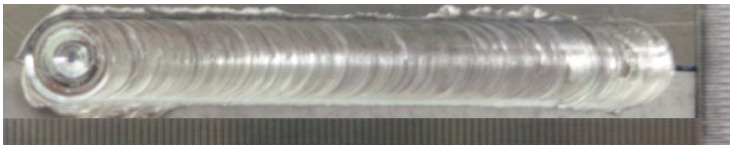
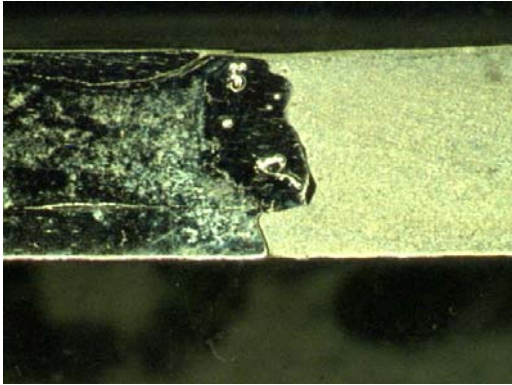
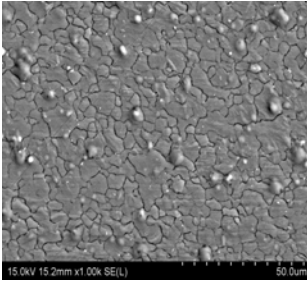
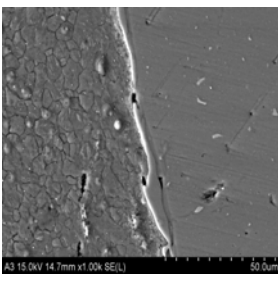
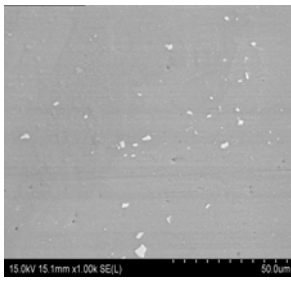
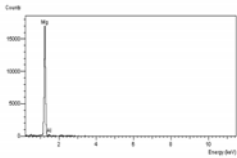
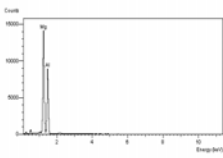
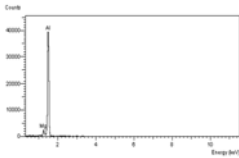
# 52 Bead			
Cross section			
SEM			
EDS			



Table 4.6 Micro-structure observation of condition number 59

# 59 Bead			
Cross section			
SEM			
EDS			

## 4.5 Consideration about Experiment

### – Result of welding residual stress measurement

- i) The welding residual stresses from numerical analysis and the measured welding stresses are seen distributed almost in similar pattern.
- ii) It is revealed that the maximum stresses, measured in similar weldments, are generated similarly at both sides of center axis but the maximum stress is generated on the side of Al6061-T6. Though the experimentally and numerically obtained residual stress are in similar manner, the measured residual stresses is higher than the analyzed stresses.

### – Mechanical tests and micro-structure examination

- i) From the result of tensile test, it is found that the fracture is generated at weld zone, slightly away from weld line in all specimens.  
Many thesis has been reported that types of Al materials should be located at retreating side but the graph in this thesis shows that adverse case also is necessary to obtain optimum welding condition.
- ii) The maximum value of hardness of dissimilar weldment appears in weld ment and hardness is lower in AZ31 than Al6061-T6.
- iii) SEM and EDS images shows that boundary of each material was jointed well and chemical component ratio of Al6061-T6 to AZ31 also shows balanced value.
- iv) Three separate weld specimens has been selected for hardness test and the results were compared. When comparing the hardness values of three specimens, the maximum hardness value of dissimilar weldment appeared on #52 that shown good top bead shape. The reason why hardness value of weldment appears lower than that of base metal in dissimilar welding joint is effect of different characteristics each other



and weldment grain size shows uneven state.

When summarizing the results, the experimental values shows good agreement with numerically calculated values. And in strength aspect, similar weld is superior to dissimilar weld and is proved experimentally enough .

## Chapter 5

### Conclusion

This chapter synthesizes the results,

- ◆ In this thesis, 90 trials was carried out to obtain good welding condition. Angle, tool geometry and thickness were fixed and RPM, travel speed, tool penetrating position, material position were changed according to experiment process.

As a result, good bead shape was observed below conditions

#52; 600rpm—travel speed:0.8mm/sec—penetrating position(away form  
center:0mm—tool penetrating depth:99.1mm—advancing side: Al6061—T6  
#59; 600rpm—travel speed:0.3mm/sec—penetrating position(away form  
center:0mm—tool penetrating depth:99.1mm—advancing side: Al6061—T6  
#62; 600rpm—travel speed:0.3mm/sec—penetrating position(away form  
center:2mm—tool penetrating depth:99.1mm—advancing side: Al6061—T6

- ◆ The analyzed residual stresses and the measured residual stresses distribute in similar manner but the measured residual stresses is higher than the analyzed stresses. Moreover, **measured residual stress value was fluctuated at both of base metals because specimen prepared for FSW process is thin plate(2mm)**. Commonly, thin plate is susceptible to be deformed under even low heat input condition.
- ◆ When comparing the hardness values of three specimens, **the maximum hardness value of dissimilar weldment appeared on #52** that shown good top bead shape. The reason why hardness value of weldment appears lower than that of base metal in dissimilar welding joint is effect

of different characteristics each other and weldment grain size shows uneven state.

◆ From the result of tensile test, it is found that the fracture is generated at weld zone, slightly away from weld line in all specimens, It has been noticed many thesis that Al materials should be locate at retreating side but the tensile test graph shows the adverse case and it is found necessary to obtain optimum welding condition

◆ SEM and EDS images shows that boundary of each material was joined well and chemical component ratio of Al6061-T6 and AZ31 also shows balanced value.

In this thesis, good welding condition between Al6061-T6 and AZ31 was obtained and verified by experiments and numerical analysis. Also, numerical analysis program was developed and verified by comparing experimentally measured residual stress results.

## REFERENCES

- [1] H.S. Bang, H.S. Bang, S.M. Joo, "Numerical simulation of Al-SPCC weldment", Key Engineering Materials, P1738~1744, Oct., 2006
- [2] Y.J.Chao, and X.Qi: Heat transfer and thermo-mechanical analysis of Friction Stir joining of Al6061-T6 plates, 1st International Symposium on Friction Stir Welding, (1999).
- [3] A.Askari, S.Silling, B.London, and M.Mahoney: Modelling and Analysis of Friction Stir Welding Processes, Friction stir welding and Processing, TMS publication,(2001) p.43.
- [4] A.William, Using Gleeble flow stress data to establish optimum FSW processing parameter in Aluminium Alloys, Advanced material processing centre, (2002).
- [5] H.S. Bang. "Study on The Mechanical Behaviour of Welded part in thick Plate - Three-dimensional Thermal Elasto-Plastic Analysis Baseon Finite Element Method." Journal of the Korean Welding Society, Vol.10, No.4, pp.37~43, December 1992.
- [6] Rajesh S.R., "Development of mathematical model for Thermo-mechanical behavior of Friction Stir Welding an introduction Soldering by using FEM/BEM", 2007
- [7] G.Comini, S.D.Giudice, and C.Nonino: Finite Element Analysis in Heat Transfer Taylor & Francis,Italy,(1994).
- [8] H.S. Bang and Y.C. Kim. "Analysis on The Three-Dimensional Unstationary Heat Conduction on The Welding of Thick Plates by F.E.M." Journal of the Korean Welding Society, Vol.9, No.2, pp.37~43, Jun 1991.
- [9] Bynum, J.E., "Modification to the Hole Drilling Technique of Measuring Residual Stresses for Improved Accuracy and Reproducibility", Journal of Experimental Mechanics, U.S.A., Vol. 21, No. 1, Jan. 1981.

- [10] AWS, WELDING HANDBOOK, Vol.1, Eighth Edition, 1987.
- [11] AWS, WELDING HANDBOOK, Vol.2, Eighth Edition, 1991.
- [12] Jianxun Zhang and Hidekazu Murakawa, "FEM Simulation of welding process (Report II)", Trans. JWRI, Vol. 27, No. 2, pp.73~79, 1998.
- [13] Hidekazu Murakawa, Jianxun Zhang and Hiroyuki Minami, "FEM Simulation of welding process(ReportIII)", Trans. JWRI, Vol. 28, No.1, pp.41~46, 1999.
- [14] L.E.Murr, et al.: Solid-state flow association with the friction stir welding of dissimilar metals, Fluid flow phenomena in metals processing (1999), 31-40
- [15] K. Chattopadhyay, et al.: "Microstructural development of dissimilar weldments: case of MIG welding of Cu with Fe filler", Journal of materials science 37 (2002) 2345-2349
- [16] C. Maldonado, T. H. North, " Softened zone formation and joint strength properties in dissimilar friction welds", Journal of materials science 37 (2002) 2087-2095
- [17] Z. Sun, R. Karppi, "The application of electron beam welding for the joining of dissimilar metals: an overview", Journal of materials processing technology 59 (1996) 257-267
- [18] H.S. Bang, G.Y. Han, "The plane-deformation thermal elasto-plastic analysis during welding of plate", The society of naval architects of korea p33~40, Apr.1994
- [19] COLIN J. SMITHELLS, Metals Reference Book, FIFTH EDITION, BUTTERWORTHS, pp.942, pp.952, 1976.
- [20] S. Katayama, et al.: Proc.5th Int.Conf.on TRENDS IN WELDING RESEARCH, Georgia, June (1998), pp.467-472.

- [21] WELDING HANDBOOK, Eighth Edition, Volume 3, MATERIALS AND APPLICATION PART 1, pp.100~110, AMERICAN WELDING SOCIETY.
- [22] E. G. WEST, THE WELDING OF NON-FERROUS METALS, CHAPMAN & HALL LTD, 1951, pp.129~254.
- [23] R.T. Jones, Q.G. Reynolds, M.J. Alport. "DC arc photography and modelling."Minerals Engineering , Vol. 15, pp.985~991, 2002.
- [24] Thermal stress, creep and heat conduction analysis by finite element method, Science, pp.1~99, pp.115~120, pp.135~158, 1985. (in Japanese)
- [25] KOICHI MASUBUCHI, Analysis of Welded Structure, PERGAMON PRESS, pp.1~234, 1980
- [26] D. R. J. OWEN and E. HINTON, FINITE ELEMENTS IN PLASTICITY: Theory and Practice, Pineridge Press Limited, pp.13~31, pp.215~269, 1980.
- [27] JOHN GOLDAK, ADITYA CHAKRAVARTI, and MALCOLM BIBBY. "A New Finite Element Model for Welding Heat Sources."METALLURGICAL TRANSACTION B, VOLUME 15B, pp.299~305, JUNE 1984.
- [28] Hidekazu Murakawa and Jianxun Zhang, "FEM Simulation of welding process (Report I )", Trans. JWRI, Vol. 27, No. 1, pp.75~82, 1998.
- [29] H.S. Bang. "Study on The Mechanical Behaviour of Welded part in thick Plate - Three-dimensional Thermal Elasto-Plastic Analysis Base on Finite Element Method." Journal of the Korean Welding Society, Vol.10, No.4, pp.37~43, December 1992.

## Acknowledgments

여기 작은 결실의 순간을 정리하는 지금, 너무나도 많은 분들의 도움에 감사의 마음을 담아봅니다.

저에게 지난 2년의 시간은 인생의 큰 전환점이자, 너무나 짧고 힘들었던 시간이었습니다. 그러나 이러한 시간이 크나큰 행복임을 일깨워주시고 “배움”이 얼마나 가치 있고 사람을 변화 시킬 수 있는지를 가르쳐주신 방한서 교수님에게 형용할 수 없는 존경심과 감사함을 전하고 싶습니다. 또한 지도와 관심을 베풀어주신 방희선 교수님과 김도정 교수님, 이창우 박사님께 심심한 감사의 마음을 전합니다.

직장 다니며 졸업논문 준비한다는 것이 너무나 힘들었지만 연구실 후배들이 있어 이러한 행복한 순간을 맞이할 수 있었습니다. 형을 대신해 인장시험 하라 고생한 근홍이, SEM과 EDS 때문에 발바닥 불난 현종이, 경도측정 하라 고생한 현수와 세민이, 잔류응력측정 하라 고생한 용혁이, 그리고 공청회 준비해 도움준 주연이, 정미, 준형이, 그리고 영문논문에 조언을 준 Bijoy와 실험 방법에 아낌없는 조언을 해준 Rajesh 모두 감사드립니다.

또한 회사에서 논문준비하며, 많은 조언을 주신 창수형님과 호경형님에게 감사드리며, 그 외에 심적으로 걱정해주신 사무실의 동료 여러분과 많이 부족하지만 Class Surveyor로써 첫걸음을 인도해주신 이수영지부장님께 깊은 감사드립니다.

마지막으로 저를 세상에 나게 해주시고 항상 믿어주신 아버님과 어머니, 그리고 사랑으로 감싸준 형과 동생모두 너무 고맙습니다.

너무나 값진 시간과 행복한 기억을 맘속에 고이 담고서

2009년5월29일 새벽에

구조용접연구실에서

손 창 식 올림

## 후 기

이 논문(저서)은 2007년 정부(교육인적자원부)의 재원으로 한국 학술 진흥재단의 지원을 받아 수행된 연구(KRF-2007-D00301) "2007 문제해결형 인력양성지원\_이공계 석/박사과정생 - 마찰교반용접(FSW)을 이용한 이종재료(알루미늄 합금/마그네슘합금)의 접합특성" 에 의해 수행된 연구 결과이며 관계자 여러분께 감사드립니다.



## 저작물 이용 허락서

학 과	선박해양공학과	학 번	20077567	과 정	석 사
성 명	한글: 손 창 식    한문 : 孫 昌 植 영문 : <b>Chang-Sik Son</b>				
주 소	광주광역시 남구 주월2동 1048-35 3/3				
연락처	E-MAIL : <b>chang-sik.son@lr.org</b>				
논문제목	한글 : 마찰교반용접을 이용한 이종합금재료 (Al6061-T6 + AZ31)의 기계적 특성에 관한 연구 영문 : A study on the Mechanical Characteristics in Dissimilar (Al / Mg) Alloy by using Friction Stir Welding				

본인이 저작한 위의 저작물에 대하여 다음과 같은 조건아래 조선대학교가 저작물을 이용할 수 있도록 허락하고 동의합니다.

- 다 음 -

1. 저작물의 DB구축 및 인터넷을 포함한 정보통신망에의 공개를 위한 저작물의 복제, 기억장치에의 저장, 전송 등을 허락함
2. 위의 목적을 위하여 필요한 범위 내에서의 편집·형식상의 변경을 허락함. 다만, 저작물의 내용변경은 금지함.
3. 배포·전송된 저작물의 영리적 목적을 위한 복제, 저장, 전송 등은 금지함.
4. 저작물에 대한 이용기간은 5년으로 하고, 기간종료 3개월 이내에 별도의 의사표시가 없을 경우에는 저작물의 이용기간을 계속 연장함.
5. 해당 저작물의 저작권을 타인에게 양도하거나 또는 출판을 허락을 하였을 경우에는 1개월 이내에 대학에 이를 통보함.
6. 조선대학교는 저작물의 이용허락 이후 해당 저작물로 인하여 발생하는 타인에 의한 권리 침해에 대하여 일체의 법적 책임을 지지 않음
7. 소속대학의 협정기관에 저작물의 제공 및 인터넷 등 정보통신망을 이용한 저작물의 전송·출력을 허락함.

동의여부 : 동의( ☒ )    반대( ☐ )

2009년 5월 일

저작자: 손 창 식 (서명 또는 인)

조선대학교 총장 귀하